PHILOSOPHICAL TRANSACTIONS OF THE ROYAL SOCIETY A MATHEMATICAL, PHYSICAL & ENGINEERING SCIENCES

A Precision Determination of the Lamb Shift in Hydrogen

G. Newton, D. A. Andrews and P. J. Unsworth

Phil. Trans. R. Soc. Lond. A 1979 **290**, 373-404
doi: 10.1098/rsta.1979.0004

A PRECISION DETERMINATION OF THE LAMB SHIFT IN HYDROGEN

BY G. NEWTON,* D. A. ANDREWS† AND P. J. UNSWORTH*

* *School of Mathematical and Physical Sciences, The University of Sussex, Brighton, BN1 9QH, U.K.*

† *Department of Physics, Schuster Laboratory, The University, Manchester, M13 9DL, U.K.*

(*Communicated by R. J. Blin-Stoyle, F.R.S. – Received* 13 *April* 1978)

CONTENTS

Vol. 290. A 1373. 35 [Published 29 January 1979

For over 40 years, optical and microwave spectroscopists, and atomic, nuclear and elementary particle physicists have been engaged in measuring the $2^2S_{\frac{1}{2}}$–$2^2P_{\frac{1}{2}}$ energy level separation in atomic hydrogen (the Lamb shift) and attempting to predict the splitting theoretically. The discrepancies encountered have influenced the development of theoretical methods of calculation in the areas of atomic structure, quantum electrodynamics and elementary particle physics.

In this paper we present the results of a precision microwave determination of the Lamb shift, using a fast atomic beam and a single microwave interaction region. The value obtained is in substantial agreement with the earlier determinations and with the recent calculation by Mohr but is in disagreement with the earlier calculation by Erickson. This disagreement is further accentuated if recent modifications to the size of the proton are included, whereas the agreement with Mohr's calculation is not affected.

The experimental method uses a 21 keV beam of metastable 2s hydrogen atoms which are obtained by charge exchange of a proton beam extracted from a radio frequency (r.f.) ion source. The experiment is performed in essentially zero magnetic field and uses a precision transmission line interaction region to induce r.f. transitions at the Lamb shift frequency. The result for the $2^2S_{\frac{1}{2}}$ $F = 0$ to $2^2P_{\frac{1}{2}}$ $F = 1$ interval in zero field is 909.904 ± 0.020 MHz corresponding to a Lamb shift of 1057.862 ± 0.020 MHz.

The paper discusses the method and the host of corrections for systematic effects which need to be applied to the line centre, many of which have not been sufficiently understood or controlled in previous experiments. The paper is introduced with a brief survey of significant landmarks in calculation and measurement of the Lamb shift and concludes with a comparison of the present theoretical and experimental positions.

1. Introduction

In the development of quantum mechanics and quantum electrodynamics, studies of atomic hydrogen have played a crucial role; since only a single electron and proton coupled by the radiation field are involved, the dynamics is amenable to precise calculation which may be compared directly with experimental measurements. The difficulties in reconciling theoretical predictions with experimental results have acted as an effective stimulus to the development and improvement of both theoretical models and experimental methods. This paper describes an experimental measurement of the Lamb shift in hydrogen and discusses the host of corrections for systematic effects which have to be applied to the result.

The experiment is introduced with a brief survey of significant landmarks in the discovery, calculation and measurement of the Lamb shift in hydrogen, and concludes with a comparison of the present theoretical and experimental positions.

1.1. *Discovery and calculation of the Lamb shift*

In the original treatment of Bohr (1913), the differing degrees of ellipticity associated with the allowed orbits for a given principal quantum number n, were not expected to contribute a fine structure to the energy of the state E_n. In contrast, Michelson & Morley had shown through spectroscopic evidence in 1887 that such a fine structure did exist. However it was soon shown by Bohr (1915) and Sommerfeld (1916) that the relativistic variation of the electron mass with velocity would allow for a dependence of the energy on the eccentricity of the orbits, and so remove the degeneracy predicted by the earlier theory. For the $n = 2$ states in hydrogen one orbit is circular and the other elliptical, and the calculated energy difference

$$\Delta E = \tfrac{1}{16}\alpha^2 hc\,\mathrm{Ry} = 0.365\ \mathrm{cm}^{-1}$$

is in agreement with experiment and the later Dirac (1928) theory. Early applications of relativistic wave mechanics were unsuccessful in calculating the energy difference between these two orbits, and it was not until the *ad hoc* addition of electron spin and magnetic moment postulated by Goudsmit & Uhlenbeck (1926) that wave mechanical methods were successful. The theory of Dirac gave the same energy levels and fine structure as the revised wave mechanics with spin and relativistic corrections, but made fewer *ad hoc* assumptions. It predicted degeneracy for states with the same n and j, but subsequent experiments failed to confirm this degeneracy, and this played a major part in the development of a new theory, quantum electrodynamics.

The spectroscopic investigations of the fine structure of the Hα line carried out by Houston & Hsieh (1934) and Williams (1938) showed discrepancies with predictions of the Dirac theory. Pasternack (1938) showed that these could be accounted for if the $2^2S_{\frac{1}{2}}$ energy level was raised very slightly above the $2^2P_{\frac{1}{2}}$ level. The Dirac theory does not predict such a splitting of the $2^2S_{\frac{1}{2}}$ and $2^2P_{\frac{1}{2}}$ energy levels, and it was the opinion of Drinkwater *et al.* (1940), in view of the extreme difficulty of the experiment and smallness of the discrepancy (10 % of the $2^2P_{\frac{1}{2}}$–$2^2P_{\frac{3}{2}}$ fine structure separation), that there was insufficient evidence of a real discrepancy. It was not until the precision microwave measurements of Lamb & Retherford (1947) and Lamb *et al.* (1950–1953) that the $2^2S_{\frac{1}{2}}$ and $2^2P_{\frac{1}{2}}$ states were shown unambiguously not to be degenerate, but to be split by about 0.03 cm^{-1} in agreement with Pasternack's suggestion. Confirmation of the Lamb–Retherford result was obtained from spectroscopic measurements by Mac & Austern (1947, 1950), Kopferman *et al.* (1949), Murakawa *et al.* (1949), and Kuhn & Series (1950).

The splitting is absent in the Dirac theory because the interaction of the electron with the radiation field is not fully taken into account. Welton (1948) has shown that the bulk of the Lamb shift, as the splitting is called, can be accounted for by assuming that the zero point fluctuations of the radiation field cause the electron to vibrate in its orbit and so smear out its effective charge. This modifies the avergae potential energy of the electrostatic interaction between the electron and the nucleus in the strongly varying region within and around the nucleus. Since S states have a higher probability of penetrating the nucleus than P states, they are more affected and so become shifted relative to the P state.

More rigorous approaches to the calculation of the quantum electrodynamic effects have been undertaken by Bethe (1947), Salpeter (1953), Erickson & Yennie (1965), Appelquist & Brodsky (1970), Erickson (1971) and Mohr (1975), to name but a few.

PHILOSOPHICAL TRANSACTIONS OF THE ROYAL SOCIETY A MATHEMATICAL, PHYSICAL & ENGINEERING SCIENCES

1.2. *Previous experiments*

Before we describe our method in detail it is worthwhile to review briefly the methods used in previous precision experimental determinations of the Lamb shift interval; this will provide an historical background and show the reader why the earlier investigations were unable to exploit the techniques used by Lundeen & Pipkin (1975) and Andrews & Newton (1976*a*). The first experimenters to show conclusively that the $2^2S_{\frac{1}{2}}$, $2^2P_{\frac{1}{2}}$ levels are not degenerate were Lamb & Retherford (1947). They used an atomic beam of metastable $2^2S_{\frac{1}{2}}$ atoms, and measured the $2^2S_{\frac{1}{2}}$–$2^2P_{\frac{1}{2}}$ splitting by determining the frequency of microwave electromagnetic radiation which stimulated transitions into the unstable $2^2P_{\frac{1}{2}}$ state which decays with a mean lifetime of 1.6×10^{-9} s to the ground state. The fraction of atoms decaying due to microwave transitions (the beam 'quench') was measured by monitoring the atoms which survived in the $2^2S_{\frac{1}{2}}$ state to reach a detector beyond the microwave interaction region. To scan the microwave resonance one can, in principle, either (i) vary the frequency of the microwave perturbation and record the quench as a function of frequency, or (ii) apply a variable magnetic field to cause a Zeeman shift which sweeps the atomic transition through resonance with a fixed microwave frequency, and record the quench as a function of magnetic field. Because of the technical difficulties in maintaining the strength of the microwave perturbation constant as the frequency is varied, Lamb & Retherford chose alternative (ii). The $2^2S_{\frac{1}{2}}$–$2^2P_{\frac{1}{2}}$ interval can now be found by extrapolating to zero field and making corrections to allow for the hyperfine structure. A full and detailed account of the work of Lamb and his co-workers is to be found in Lamb *et al.* (1950–1953).

About a decade later an independent series of measurements of the Lamb shift was made by Robiscoe (1965) and Robiscoe & Cosens (1966). They used the level crossing technique in which the Zeeman effect is used to shift certain hyperfine components of the $2^2S_{\frac{1}{2}}$ and $2^2P_{\frac{1}{2}}$ levels until they become degenerate. A small constant electric field is applied simultaneously to mix the $2^2S_{\frac{1}{2}}$ metastable state with the short-lived $2^2P_{\frac{1}{2}}$ state. For a given electric field, the mixing increases as the energy separation of the levels is decreased and reaches a maximum when the levels become degenerate at the crossing point. Both levels are then short-lived and maximum quench (decay) of the beam is observed. The Lamb shift interval can be deduced from the crossing point and known Zeeman shifts of the two levels.

The sensitivity of the $2^2S_{\frac{1}{2}}$ metastable lifetime to applied electric fields can lead to serious systematic errors and hence methods employing large magnetic fields suffer because the moving atoms experience a relativistic (motional) electric field $(\boldsymbol{v} \wedge \boldsymbol{B})/c$ which causes a velocity- and field-dependent decay (quenching) of the metastable state in competition with the microwave or level crossing transitions. Stray electric fields from surface charges on the apparatus can also affect the observed quench. The difficulty in estimating the correction due to these effects caused Robiscoe twice to revise his measured value of the Lamb shift (by 0.19 MHz (Robiscoe 1968) and by +0.04 MHz (Robiscoe & Shyn 1970)), and to suggest that the Lamb *et al.* (1953) value might be in error by up to 0.1 MHz.

One of the main obstacles to a precision measurement is the large natural line width (100 MHz) of the 2S–2P transition arising from the short lifetime of the 2P state. Hughes (1960) pointed out that a considerably narrower interference line shape would result if the Ramsey (1956) separated field technique could be used. This replaces a single radio-frequency interaction region by two separated regions fed coherently from the same microwave source. Beam atoms interact suc-

cessively with the coherent microwave field in each region and yield a line shape analogous to a two slit interference pattern. Hughes suggested using a fast metastable $2^2S_{\frac{1}{2}}$ beam obtained by charge exchange of a 10–100 keV proton beam, and Lundeen & Pipkin (1975) reported a successful experiment. They achieved a threefold reduction in line width, and a corresponding increase in the precision of the measurement; and further, unlike previous investigators, their experiment was carried out in essentially zero magnetic field so eliminating the troublesome $(\boldsymbol{v} \wedge \boldsymbol{B})/c$ quench. This latter feature was made possible largely by the very considerable advances in microwave technology which allowed them to scan directly the atomic interval by varying the frequency of the microwave perturbation, and at the same time hold the microwave amplitude constant to sufficient accuracy (1 part in 10^4 over a 20 % frequency change).

In the period between the publication of the results of Robiscoe (1965) and Lundeen & Pipkin (1975), the present authors (Newton *et al.* 1975) investigated a technique which eliminated both the magnetic and microwave fields. We sent a fast beam of metastable atoms through a region in which an electrostatic field periodically reverses in space along the beam axis. During their passage through such a region, the atoms experience a field oscillating at a frequency determined by their velocity and the electrode spacing. The atomic resonance is then observed by measuring the quench as a function of beam velocity. We concluded that while this method could yield results competitive with those of Lamb *et al.* and Robiscoe *et al.* it was unlikely, even after considerable refinement, to be competitive with the new microwave techniques. Our precision measurement was made therefore using a microwave method.

2. The experimental method

Though the separated microwave field method produces an interference signal whose line width can be made significantly narrower than that obtained by the single field method, it has the disadvantage of a greatly reduced signal strength. When one of the atomic states can decay by spontaneous radiation, the interference signal decreases exponentially with the time spent between the microwave regions, whereas the 'interference narrowing' is proportional to the time. Hence it is not practical to attempt to narrow the line by more than a factor of 3 to 5. The significant loss of signal strength, increased complexity of the apparatus and line shape and the non-adiabatic passage of the atoms are features which can contribute systematic errors and have to be weighed against the advantage of the reduced line width.

For these reasons we have used a single microwave region in the form of a 50 Ω transverse transmission line with a beam of kinetic energy 21 keV which is slow enough to ensure an adiabatic switch-on and -off of the perturbation. Further, since the solutions of Maxwell's equations for the particular transmission line geometry chosen can be obtained analytically, a precise description of the spatial distribution of the field exists, so enabling the atomic and instrumental line shape to be calculated precisely. This is of prime importance in the testing and interpretation of the observed resonance line shapes.

In outline the experimental method and apparatus are as follows (see figure 1). A radio-frequency ion source is used to produce a beam of protons which are accelerated and focused into a quasi-parallel beam which passes through a gas cell. During their passage through the cell a portion of the protons capture an electron and emerge in the form of a fast, well collimated beam of hydrogen atoms in all possible excited states and the ground state. Within a short time (0.5 μs) most of the excited states have decayed, leaving the beam composed mainly of ground

state and metastable 2 s atoms. A radio-frequency state selector is then used to induce transitions which leave only one particular 2s hyperfine level populated.

This additional state selection is desirable since it considerably simplifies the subsequent line shape obtained. The main microwave resonance region consists of a 50 Ω transmission line ('slab line') positioned so that the microwaves propagate in a direction perpendicular to the motion of the beam to eliminate first order Doppler shifts. The surviving metastable atoms

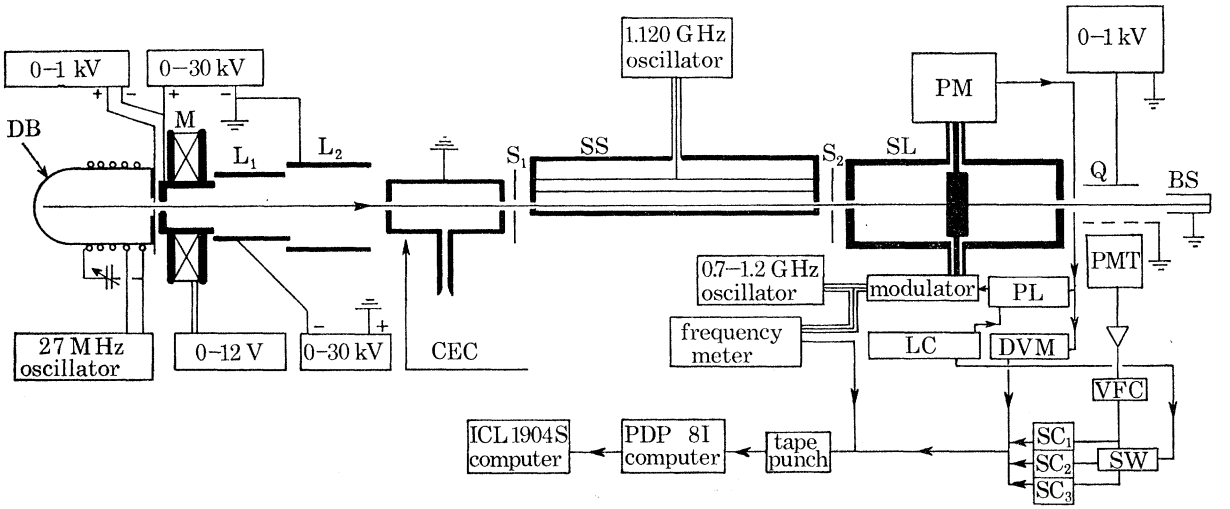

FIGURE 1. Schematic of apparatus. DB, quartz discharge bulb; M, electromagnet (1000 amp turns); L_1 and L_2, electrostatic lenses; CEC, charge exchange cell cooled with liquid nitrogen; S_1 and S_2, beam collimating slits; SS, coaxial radio-frequency state selector; SL, 50 Ω transverse slab line; PM, microwave power meter; Q, metastable beam quencher; BS, beam stop; PL, microwave power leveller; LC, logic control and clock; DVM, digital voltmeter; VFC, voltage to frequency converter; SW, signal switch; SC_1, SC_2 and SC_3, scalers; PMT, photomultipler tube.

emerging from the slab line are detected with a ultraviolet photomultiplier and the resulting signal is recorded by use of digital techniques. To observe the resonance, the quench is measured as a function of microwave frequency and the line centre is obtained by fitting to the theoretical line shape. This experimental technique gives the following advantages over the various preceding methods: (i) by carrying out the experiments in the Earth's magnetic field, the troublesome effects of $(\boldsymbol{v} \wedge \boldsymbol{B})/c$ motional electric fields are greatly reduced; (ii) the analytically calculable field of the transmission line geometry used for the radio-frequency transition region gives a simple and precisely calculable line shape, in contrast to the complex interference pattern of the separated field method; (iii) high beam and signal intensities ensure good counting statistics.

3. APPARATUS

3.1. *Metastable beam source*

A hydrogen discharge is excited in a quartz bulb by a 27 MHz oscillator inductively coupled to the discharge. A Faraday electrostatic shield is fitted between the discharge vessel and the excitation coil to prevent the strong longitudinal electric field across the coil from upsetting the stability of the discharge. Two extraction electrodes placed external to the discharge produce an initially convergent beam which is subsequently accelerated and focused by a three-element cylindrical lens (Liebmann 1949). To achieve a high proton fraction in the beam (96 %), the

molecular recombination rate on the walls of the discharge vessel must be small. Smith (1943) has shown that the recombination coefficient for metal surfaces is approximately unity whereas for Pyrex and quartz it is of the order of 10^{-5}–10^{-4}. For this reason the electrode that defines the plasma potential is covered with a quartz disk, except for a small area of 2 mm² in the neighbourhood of the orifice, where it is in direct contact with the plasma. For a full and detailed description of the ion source the reader is referred to Newton & Unsworth (1975).

The charge exchange cell is approximately 5 cm long by 1 cm in diameter and is fitted with small apertures at each end to allow the beam to enter and leave. Gas is admitted through a side arm, and, to reduce the flow rate into the adjacent vacuum system, the end apertures are in the form of tubes whose length is five times their diameter. To reduce the flow further the cell is cooled with liquid nitrogen. Ar, N_2 and H_2 were tried as gas targets, but hydrogen yielded the strongest metastable beam in spite of its small charge exchange cross section. This is thought to be due to the greater large-angle scattering associated with the heavier targets.

3.2. *Detector*

To detect the metastable $2^2S_{\frac{1}{2}}$ atoms, the beam is passed through a strong static electric field, which admixes a component of the short-lived $2^2P_{\frac{1}{2}}$ state into the $2^2S_{\frac{1}{2}}$ state wavefunction, and causes the beam atoms to decay ('quenches' the beam) with the emission of Lyman-α radiation ($\lambda = 0.1216\,\mu m$). The emitted Ly-α radiation strikes the first dynode of an electron multiplier, and the photoelectric current generated is amplified by the subsequent dynodes in the normal manner. For efficient collection of Ly-α photons, the quenching field must be restricted to a region within the field of view of the 'photocathode'. This is achieved by positioning a set of coaxial electrodes in front of the electron multiplier so that it 'looks' along the axis of the assembly. Small apertures are cut in the outer electrode to allow the beam to pass transversely through the structure. A cleaved LiF window is placed directly in front of the photocathode to prevent the entry of charged particles produced by collisions between the fast beam and the residual atoms and molecules in the evacuated (2×10^{-8} Torr) detector chamber.

The amplified photoelectric current leaving the anode is further amplified by a temperature stabilized F.E.T. operational amplifier, before passing to a voltage to frequency convertor (Unsworth 1969) and thence to a system of gated scalers. The gating is synchronized to the switching of the microwave power so that the beam strength can be recorded with and without induced microwave transitions. A typical switching rate and scalar integration time are 120/s and $5\frac{1}{2}$ min respectively. Linearity to better than 1 in 10^4 during the voltage to frequency conversion is ensured by introducing an integration time constant of 1 ms in the F.E.T. amplifier, to limit the current fluctuations to be not greater than the dynamic range of the converter. The effect of this and other time constants on the quench values was minimized by introducing a 'dead time' in the counting for 3 ms after switching the r.f. power on or off.

3.3. *Interaction region*

In order to produce undistorted line shapes capable of determining the Lamb shift to the required accuracy, it is necessary to control the r.f. power applied very carefully. If the power varied with frequency across the resonance, this would shift the apparent centre of the line. For instance, a variation of only 0.1 % in absolute power across the full width of the resonance (100 MHz) would produce a substantial shift of 25 kHz. At frequencies around 1 GHz the only feasible method of applying r.f. power in a sufficiently controlled manner is to use a transmission

line and a matched load to absorb the power. Even so, the effects of standing waves due to slight impedance mismatches are of great importance, and are considered in detail in § 5.7. In the system used, the matched load is also the power measuring device, namely a precision 10 dB General Radio attenuator and a Hewlett–Packard 50 Ω load and power sensor type 8481A. The atomic beam is passed through the transmission line structure at right angles to the r.f. propagation direction to eliminate first-order Doppler shifts in frequency. With no standing waves present the field experienced by the atoms is independent of frequency.

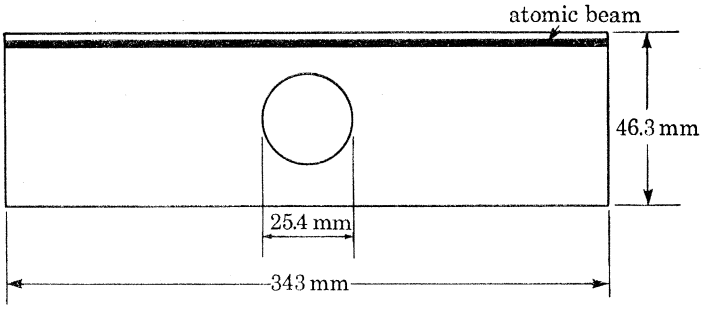

FIGURE 2. Section through slab line showing position of beam relative to conductors.

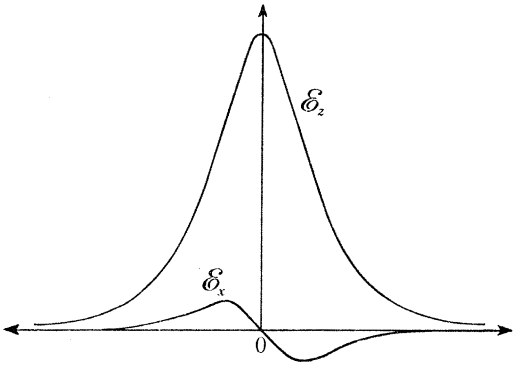

FIGURE 3. Electric field components as seen by the beam. The component parallel to the beam velocity reverses direction.

The transmission line geometry chosen is the so-called 'slab line' (Wholey & Eldred 1950), which consists of a cylindrical centre conductor midway between two flat plates (the outer conductor). These plates are joined together at an appropriately large distance away from the centre conductor to form a rectangular tube. A cross section through the line is shown in figure 2. The atomic beam enters from the side and travels close to the top plate in the gap between the conductors. The electric field experienced by the atom (see appendix) is shown in figure 3, and is seen to be large only near the centre bar and quite negligible at the edges of the region. In fact, it may be shown that the beam entrance ports do not influence the electrical performance of the line in any substantial way; this is an advantage that the slab line has over, for instance, the coaxial line.

In order to be able to use high precision General Radio GR 900 components, it was necessary to design a precision, wide-band coaxial to slab line converter. This takes the form of a stepped transition, using a section of high impedance line, to neutralize both real and imaginary parts of the reflexions caused by discontinuity capacitances (Whinnery *et al.* 1944). The centre con-

ductor is held in place by a compensated PTFE support which also serves as a vacuum seal allowing the line to be evacuated. The connector assembly and vacuum seal is shown in figure 4. All the dimensions are critical to ensure perfect impedance matching.

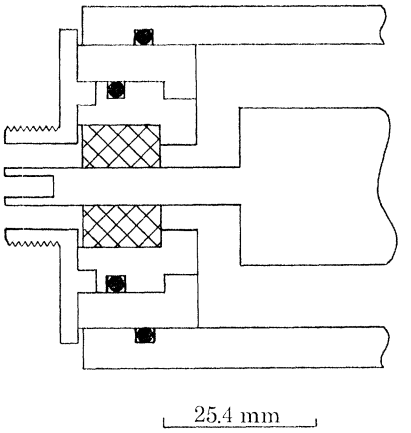

FIGURE 4. Detail of coaxial to slab line transformer and vacuum seals. The shaded central portion denotes the p.t.f.e. support/vacuum seal.

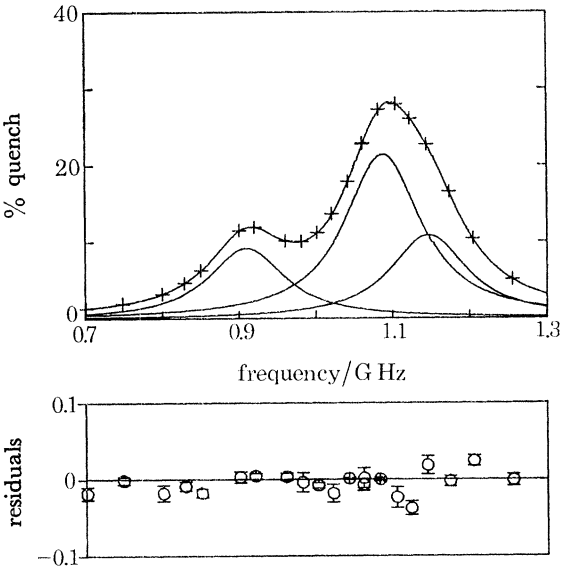

FIGURE 5. Resonance line shape in the absence of state selection. The lower portion shows the residuals after fitting the experimental points.

3.4. *Radio-frequency state selector*

A frequency scan over the possible $2^2S_{\frac{1}{2}}$–$2^2P_{\frac{1}{2}}$ transitions would produce a line shape as shown in figure 5. As can be seen, this line shape is comparatively broad, about 300 MHz, because it is composed of three overlapping resonances α, β and γ (see figure 6), each of which has a natural width of 100 MHz and a frequency separation of similar magnitude. Such a line shape is far from ideal since the precision to which any one of the α, β or γ line centres can be determined in the presence of signal noise is inversely proportional to the square of the line width. However, it is possible to simplify and narrow the line shape by first depopulating the $2^2S_{\frac{1}{2}}$ $F = 1$ state by

stimulating β and γ transitions to the short-lived $2^2P_{\frac{1}{2}}$ levels. Owing to the large natural line width of the $2^2P_{\frac{1}{2}}$ levels it is possible simultaneously to stimulate both the β and γ resonances by using a single microwave oscillator tuned to 1120 MHz without substantially affecting the $F = 0$ population. The resulting line shape is shown in figure 7.

The state selector employs a 100 Ω coaxial transmission line, centre-fed from a 50 Ω source

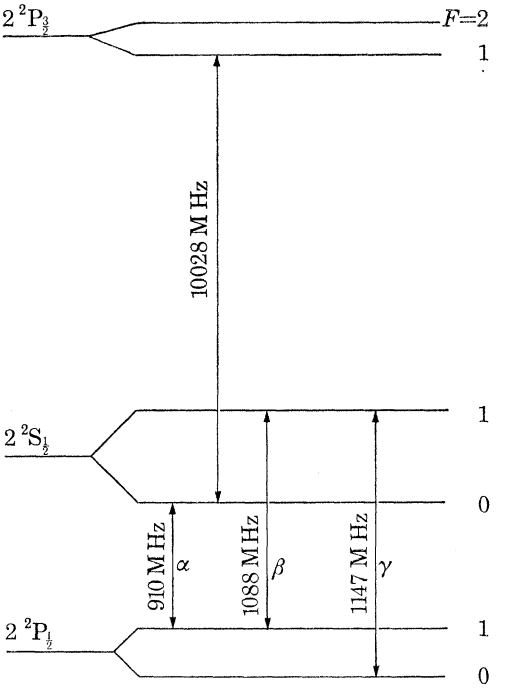

FIGURE 6. Main features of the $n = 2$ manifold in atomic hydrogen. The frequency intervals are taken from Brodsky & Parsons (1967, 1968) and rounded to the nearest MHz.

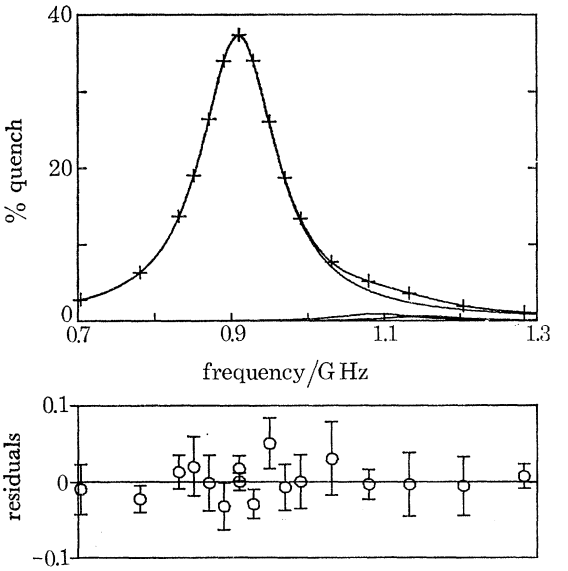

FIGURE 7. Resonance line shape obtained with state selector operating.
The lower portion shows the residuals after fitting the data. Run H from table 2 is shown.

and terminated at each end. Power from the oscillator divides at the centre and is absorbed by 100 Ω resistors. Apertures cut in the end caps allow for the passage of the atomic beam parallel to the axis. This configuration provides a small improvement in the frequency match between the oscillator frequency and the β and γ resonances because the atoms experience a splitting in the oscillator frequency due to upward and downward Doppler frequency shifts of 8 MHz.

4. Experimental procedure

4.1. *Data collection*

The experimental procedure is thus to measure the induced radio-frequency quench at a series of different frequencies between 700 and 1300 MHz. Each day's runs were preceded by a 2–3 h warm up period with the beam on to allow the oscillators and amplifiers to come to thermal equilibrium, and the ion source to clean up and evaporate adsorbed water, etc. The state selector power was then adjusted to remove 80 % of the total metastable beam, thus reducing the $F = 1$ to $F = 0$ population ratio from 3:1 to 0.02:1. The r.f. power for the Lamb shift transition region was measured by the power meter and digital voltmeter, and was kept constant to a few parts in 10^4, by means of an electronic servo system using a p–i–n diode modulator.

The frequency measurement was performed using a Hewlett–Packard 2590A frequency convertor and 5245L/5253B counter. During each counting period the frequency drifted by up to 10 kHz, and was also sensitive ($\pm$ 20 kHz) to oscillator loading (see § 5.12). At the end of each counting period, the contents of the scalers were read automatically on to punched paper tape, which was fed directly into a teletype linked to a PDP-8 computer. This computed the r.f. quench $q = (I_0 - I)/I_0$, where I and I_0 are the contents of the scaler integrating the signal with the r.f. on and off respectively. A third scaler counting during both periods was used to give a sum check on the readings. Each run consisted of 17 such frequency points, taken on alternate sides of the resonance to reduce the effect of drifts. The total time taken for each run was about 1½ h, and in all 32 runs contributed to the final result. A typical run together with its residual after fitting to the theoretical line shape is given in figure 7.

4.2. *Resonance line shape*

To obtain a value for the Lamb shift to 2 in 10^5, the centre of the resonance must be measured to better than 1 part in 2000 of the line width. This requires an accurate knowledge of the expected resonance shape so that any distortion which would cause the measured centre to be shifted can be identified and eliminated. It is therefore necessary to be able to generate theoretically precise line shapes which will match the experimental situation as accurately as possible. The way chosen to do this was to integrate numerically the Schrödinger equation for an atom in a particular state and phase ϕ relative to the r.f. field, and then average the results over the initial state populations and phase ϕ.

Within the $n = 2$ manifold of levels, the $2^2S_{\frac{1}{2}}$, $2^2P_{\frac{1}{2}}$, $2^2P_{\frac{3}{2}}$ states have 4, 4 and 8 hyperfine components respectively. However, from perturbation theory it is apparent that the $2^2P_{\frac{3}{2}}$ states contribute negligibly to the above transition probability as they are over 200 line widths away. Their only effect is to change the Bloch–Siegert shift (see § 5.2). Thus we shall neglect these levels in the integration.

The equation of state may be written in the following way:

$$i\hbar\dot{\psi} = \mathscr{H}_0\,\psi + \boldsymbol{\mu}\,.\,\boldsymbol{\mathscr{E}}(t)\,\psi, \qquad (1)$$

PHILOSOPHICAL TRANSACTIONS OF THE ROYAL SOCIETY A MATHEMATICAL, PHYSICAL & ENGINEERING SCIENCES

where $\psi(t)$ is the state vector for the atom, $\mathscr{H}_0$ the Hamiltonian in the absence of the field, $\boldsymbol{\mu}$ the electric dipole operator, and $\boldsymbol{\mathscr{E}}(t)$ the electric field actually experienced by the atom as it moves through the interaction region. By choosing axes x in the direction of the beam and y parallel to the slab line axis, the microwave field has components $\mathscr{E}_x$ and $\mathscr{E}_z$ only. If the beam is initially populated in the $2^2S_{\frac{1}{2}}\, F = 0$ state, and if the field direction remains constant, transitions only occur between the $2^2S_{\frac{1}{2}}\, F = 0$ state and the $2^2P_{\frac{1}{2}}$ states. If, however, the field direction rotates, transitions can be stimulated from $2^2S_{\frac{1}{2}}\, F = 0$ to $2^2P_{\frac{1}{2}}$ and then back to $2^2S_{\frac{1}{2}}\, F = 1$. This repopulation of the $2^2S_{\frac{1}{2}}\, F = 1$ states leads to additional line shape components at the $2^2S_{\frac{1}{2}}\, F = 1$ $2^2P_{\frac{1}{2}}$ frequencies (β and γ) and greatly complicates the line shape so making the centre less well defined. Fortunately, by arranging for the beam to travel near the top plate of the slab line where the field is everywhere nearly normal to the plate, it is possible to reduce the effect of repopulation, to an extent that the reduced (four level) matrix describes the resonance to sufficient accuracy. This was in fact verified by full eight-level computer simulations under selected conditions. Thus, for example, for the $2^2S_{\frac{1}{2}}\, F = 0\, M_F = 0$ level, the four-level equations of motion (1) take the form

$$\left.\begin{aligned} \mathrm{i}\dot{s}_{00} &= \Delta s_{00} - \tfrac{1}{\sqrt{2}} C\mathscr{E}_x p_{11} + C\mathscr{E}_z p_{10} + \tfrac{1}{\sqrt{2}} C\mathscr{E}_x p_{1-1}, \\ \mathrm{i}\dot{p}_{11} &= -\tfrac{1}{\sqrt{2}} C\mathscr{E}_x s_{00} - \tfrac{1}{2}\mathrm{i}\gamma p_{11}, \\ \mathrm{i}\dot{p}_{10} &= C\mathscr{E}_z s_{00} - \tfrac{1}{2}\mathrm{i}\gamma p_{10}, \\ \mathrm{i}\dot{p}_{1-1} &= \tfrac{1}{\sqrt{2}} C\mathscr{E}_x s_{00} - \tfrac{1}{2}\mathrm{i}\gamma p_{1-1}, \end{aligned}\right\} \tag{2}$$

where the subscripts to the coefficients s and p denote values of F and M_F, and the state vector $\psi(t)$ is

$$\begin{bmatrix} s_{00}(t) \\ p_{11}(t) \\ p_{10}(t) \\ p_{1-1}(t) \end{bmatrix}.$$

C is a constant $13.92 \times 10^6\,\mathrm{s}^{-1}\,(\mathrm{V\,cm}^{-1})^{-1}$, Δ is the Lamb shift interval ($\approx 910\,\mathrm{MHz}$) and $1/\gamma$ the P state lifetime 1.6 ns. These equations may be put into a more conveniently calculable form by substituting $\hat{s}_{00} = s_{00}\,\mathrm{e}^{\mathrm{i}\Delta t}$ and writing the state amplitudes in terms of their real and imaginary parts.

We solved the resulting set of eight coupled linear differential equations with the help of the ICL subroutine F4ODE with initial conditions $\hat{s}(0) = 1$, $p(0) = 0$, to give $\hat{s}$ and p as functions of time. The electric fields $\mathscr{E}_x$ and $\mathscr{E}_z$ are given by:

$$\mathscr{E}_i(t) = \mathscr{E}_i^0(\boldsymbol{r}_0 + \boldsymbol{v}t)\sin(wt + \phi), \quad i = x, z, \tag{3}$$

where $\mathscr{E}_x^0(\boldsymbol{r})$ and $\mathscr{E}_z^0(\boldsymbol{r})$ are the fields calculated from slab line geometry (see appendix) at position $\boldsymbol{r}$, and $\boldsymbol{v}$ is the velocity vector for the atom moving through the region. The integration path was chosen to start and end sufficiently far away from the centre bar so that a further increase in the path length did nothing to alter the value obtained for the quench

$$Q = 1 - |\hat{s}(t)|^2. \tag{4}$$

The quench Q obtained by this numerical integration of the Schrödinger equation must be averaged over the r.f. phase ϕ. Detailed numerical calculations have shown that it is sufficiently accurate to take a simple average with $\phi = 0$ and $\pi/2$ only. A typical theoretical line shape thus obtained is illustrated in figure 8.

4.3. *Fitting procedure*

Having derived a theoretical line shape, it might be thought simplest to adjust the parameters used for this simulation until the best fit to experiment is obtained. Unfortunately it is not possible to determine all the information required for such a fit to the accuracy required, and if the beam trajectory, absolute power, etc. are allowed to be free parameters, the process becomes prohibitively expensive in computer time. It is also very inefficient to have to ensure perfect fit to resonance line widths, heights, saturations, etc. if only the line centre is of real interest. To

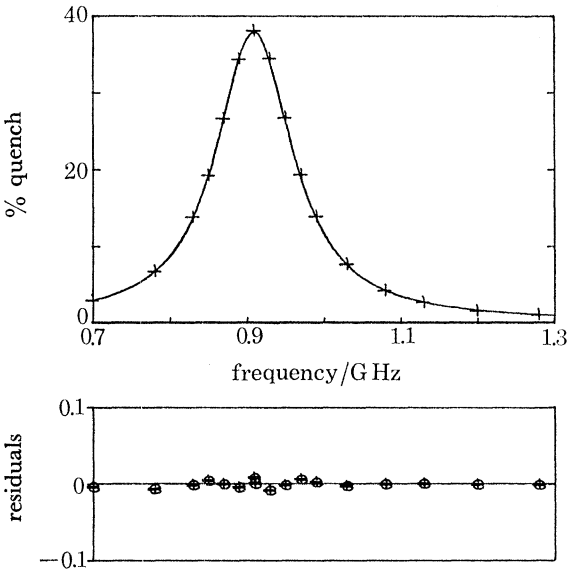

FIGURE 8. Computer simulations of the quench for microwave frequencies between 0.7 and 1.3 GHz are denoted by crosses. The full curve is obtained by fitting these points to an approximate analytical description of the line shape. The lower portion shows the residuals after fitting.

get round this problem, it was decided to look for a simple analytic function which would adequately accommodate both the theoretical and the experimental line shapes, and provide a means of comparing the two. The simplest form for such a function of the applied frequency ν would be a sum of simple lorentzians:

$$\sum_{i=1}^{3} a_i Q_i \quad \text{where} \quad Q_i = 1/(1+\lambda_i^2) \quad \text{and} \quad \lambda_i = (\nu - h_i - a_4)/a_5, \tag{5}$$

where a_1 to a_3 are free parameters corresponding to the heights of the three components α, β and γ in the line shape, h_i their (calculated) hyperfine energy shifts, and a_4 and a_5 the Lamb shift interval and half-width which are common to all three resonances. This function however is inadequate to fit the theoretical data to the required precision and must be extended in two ways: (1) an overlapping 'anti-resonance' function Q_i' due to the anti-rotating term in the Hamiltonian must be added; (2) a term must also be included to allow for the distortion of the resonance due to saturation. We have shown that these may generally be taken into account by a power series expansion in Q_i and Q_i'. The quadratic terms can be absorbed by a simple increase

in a_5, so that the next significant term is a cubic. The following empirical function was found to reproduce accurately the theoretical line shapes expected under the experimental conditions:

$$F(\nu) = \sum_i a_i[Q_i + Q_i' + a_6\{Q_i(Q_i - \tfrac{1}{2})\,(Q_i - 1) + Q_i'(Q_i' - \tfrac{1}{2})\,(Q_i' - 1)\}]$$

where
$$Q_i' = 1/(1 + \lambda_i'^2),\ \lambda_i' = (\nu + h + {}_i a_4)/a_5. \tag{6}$$

The reliability of its use to determine the Lamb shift interval a_4 from experimental data was tested on 'data' from theoretical line shapes and found to give an uncertainty in a_4 of ± 0.005 MHz. Figures 5, 7 and 8 show line shapes obtained by least squares fitting to $F(\nu)$, assuming that the residual errors are random. This last condition is obviously not necessarily true for residuals obtained from theoretical 'data' obtained from solution of the Schrödinger equation (sec § 4.2, equation (2)). However, the residuals can be used to give a reasonable estimate of the systematic error introduced by the fitting process.

In the analysis of the experimental data it was discovered that some runs showed a systematic drift in background with time. To try to eliminate this effect to first order an additional free parameter a_7 was introduced and the fitting function modified to $(1 + a_7 J)\,F(\nu)$ where J gives the serial place of the point during the run. Though χ^2 was reduced for some of the individual runs, the improvement in the experimental spread in the fitted centres compared with the six-parameter fits proved to be somewhat marginal.

4.4. *Results*

The results for the fitted line centres are summarized in tables 1 and 2. These were obtained using the full seven-parameter fit including the drift parameter a_7. In selecting the 32 runs which would contribute to the final result, we discarded only those runs which either had a grossly bad fit caused by one or two points way off the fitted curve ($> 3\sigma$, presumably due to an instrumental or operator failure), or if the fitted line centre differed from the weighted mean of all the runs by more than two of its own estimated standard deviations. The diagnosis in the second case is more difficult, but is probably due to severe background drift or fluctuations, which could not be absorbed in the drift parameter; in fact only two runs had to be rejected for these latter reasons.

TABLE 1. SUMMARY OF EXPERIMENTAL RUNS (r.f. NORMAL). Values in MHz.

run no.	measured line centre − 1050 MHz	Bloch–Siegert shift†	corrected line centre − 1050 MHz	1σ error
9B	7.875	0.086	7.789	0.056
9C	8.018	0.086	7.932	0.112
10B	7.955	0.086	7.869	0.052
10C	7.983	0.086	7.897	0.075
12B	7.917	0.086	7.831	0.034
12C	7.894	0.095	7.799	0.035
15A	7.910	0.048	7.862	0.097
15D	7.896	0.086	7.810	0.036
16A	7.938	0.086	7.852	0.053
16D	7.853	0.086	7.767	0.063
18B	7.939	0.095	7.844	0.048
18D	7.978	0.095	7.883	0.042
18F	7.882	0.095	7.787	0.027
G	7.915	0.095	7.820	0.033
I	7.920	0.095	7.825	0.029
13B	7.890	0.086	7.804	0.101
mean of runs (weighted as $1/\sigma^2$)			1057.823	0.011

† See Andrews & Newton (1976*b*).

Runs were taken approximately alternately with normal and reversed r.f. directions. Change from one configuration to the other entailed disconnecting the GR 900 connectors on the transmission line and interchanging the attenuator assembly and r.f. feed cable. Reassembly of the r.f. components produced no measurable change (0.1 %) in the voltage standing wave ratio (v.s.w.r.) thus confirming the high quality of the GR 900 connectors.

TABLE 2. SUMMARY OF EXPERIMENTAL RUNS (r.f. REVERSED). Values in MHz.

run no.	measured line centre − 1050 MHz	Bloch–Siegert shift†	corrected line centre − 1050 MHz	1σ error
8A	8.018	0.086	7.932	0.076
9A	7.831	0.086	7.745	0.090
9D	7.841	0.086	7.755	0.112
10D	8.022	0.086	7.936	0.081
12A	7.981	0.086	7.895	0.039
15B	7.917	0.048	7.869	0.086
15C	7.876	0.086	7.790	0.047
16B	7.978	0.086	7.892	0.032
16C	7.920	0.086	7.834	0.051
17B	7.875	0.086	7.789	0.066
18C	7.912	0.095	7.817	0.037
18E	7.915	0.095	7.820	0.030
F	7.965	0.095	7.870	0.036
H	7.913	0.095	7.818	0.034
J	7.913	0.095	7.818	0.042
13A	7.939	0.086	7.853	0.070
mean of runs (weighted as $1/\sigma^2$)			1057.843	0.011

† see table 1, footnote.

The weighted means obtained for the two directions are given in tables 1 and 2. The difference, due to a residual first order Doppler shift, is (20 ± 16) kHz; this would correspond to a beam misalignment of (0.19 ± 0.15) degree, which is not unreasonable. However, before we can derive a result for the Lamb shift from these results, we must first consider possible corrections to the line centre in more detail.

5. CORRECTIONS TO THE LINE CENTRE

5.1. *Hyperfine structure*

The energy level scheme is complicated in hydrogen by the presence of hyperfine structure, the $2^2S_{\frac{1}{2}}$, $2^2P_{\frac{1}{2}}$ and $2^2P_{\frac{3}{2}}$ levels each being split into doublets (see figure 9). The $2^2S_{\frac{1}{2}}$ hyperfine splitting has been accurately measured (Heberle *et al.* 1956), but the $2^2P_{\frac{1}{2}}$ splittings have to be calculated. We use formulae (8) and (9) in the treatment of Brodsky & Parsons (1967, 1968) which include radiative, relativistic and recoil corrections and the value $\alpha = 137.03604$, to obtain 59.1721 MHz for the $2^2P_{\frac{1}{2}}$ splitting. There are, in addition, off-diagonal matrix elements which couple states with the same F and l but different j; the effect of these is to lower the $2^2P_{\frac{1}{2}}$ $F = 1$ state by 2.5 kHz, by coupling to the $2^2P_{\frac{3}{2}}$ $F = 1$ state, but not to affect the other levels. We note in passing that our value for the hyperfine addition (147.9582 MHz) differs from the value quoted by Lundeen & Pipkin (147.953 MHz) by some 5 kHz, presumably due to their using the less accurate formulae given in table 2 of Brodsky & Parsons (1967).

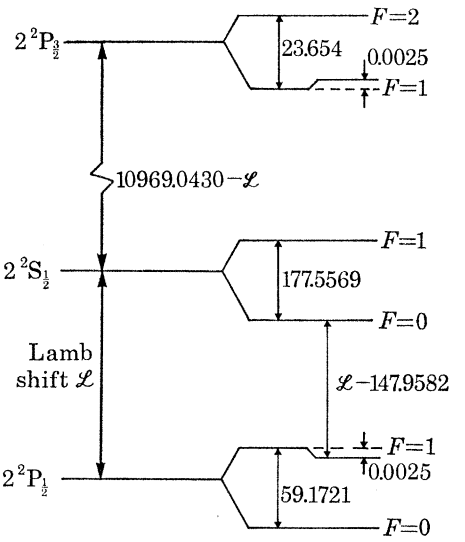

FIGURE 9. Energy level scheme of the relevant portion of the $n = 2$ manifold in atomic hydrogen. The frequency intervals have been either taken from Heberle *et al.* (1965) or calculated using formulae (8) and (9) in the treatment of Brodsky & Parsons (1967, 1968). Intervals are given in MHz.

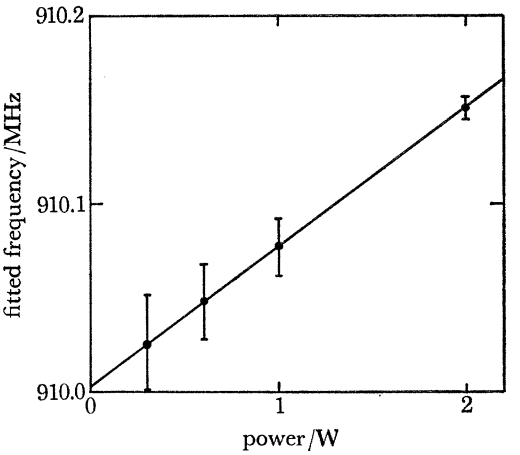

FIGURE 10. Fitted line centre as a function of the applied microwave power.

5.2. *Bloch–Siegert shifts*

The line centres found by the fitting programme for four theoretical runs with different r.f. powers are plotted in figure 10. These show a power-dependent shift which was first investigated by Bloch & Siegert (1940). We have discussed methods for calculating this shift, with special reference to the present system, in previous publications (Andrews & Newton 1975, 1976*b*); this time however we will proceed by simply fitting the points shown in figure 10 to a straight line. The resulting 'theoretical' expression for the shift derived by fitting the computed theoretical line shapes is

$$\delta\nu = 0.0712P + 0.0036\,\text{MHz}, \tag{7}$$

where P is the applied power in watts. The error in $\delta\nu$ is of the order of ± 1 kHz when P is 2 W. The constant term represents a distortion in the fitting process or in the extrapolation to zero power, or both.

An interesting check on this result is obtained from the following considerations. The Bloch–Siegert shift for a 'square pulse' of r.f. is given to first order in power by the usual expression b^2/ω (Shirley 1965) ($\hbar b$ is the matrix element of the r.f. perturbation between the states involved in the transition which has frequency ω). When, as in the slab line, the r.f. comes on and off slowly this may be generalized to the form:

$$\langle b^2/\omega\rangle = \int b^4(t))\,\mathrm{d}t/\omega \int b^2(t)\,\mathrm{d}t \tag{8}$$

With the help of the expressions given in the appendix for the slab line fields it is possible to perform these integrations analytically. The result obtained for a wide range of conditions is:

$$\langle b^2/\omega\rangle = 2b_{\max}^2/3\omega, \tag{9}$$

where $b_{\max}$ corresponds to the maximum value of b found along the trajectory. The result obtained for 2 W power agrees with equation (7) to within 1 kHz.

Various corrections need to be applied to equation (7) before it can be applied to the experimental results. The power dependent part must be multiplied by two factors: (*a*) It must be multiplied by 1.02 for the power meter calibration. (*b*) The $2^2P_{\frac{3}{2}}$ level, which is higher than the S state by approximately 10 GHz, can also be coupled by the microwave field. This non-resonant interaction produces an additional r.f. Stark effect which can be incorporated in the expression for the Bloch–Siegert shift by multiplying the power dependent term by 0.634 (see Andrews & Newton 1976*b*). Thus the net value of the radio-frequency power shift is

$$\delta\nu = 0.0460P + 0.0036\ \mathrm{MHz} \tag{10}$$

and this expression was used to correct the runs listed in tables 1 and 2. It should be noted that this shift constitutes the largest single correction applied (90 kHz).

5.3. *Stark shifts*

The $2^2S_{\frac{1}{2}}\,F = 0$ to $2^2P_{\frac{1}{2}}\,F = 1\ M_F = 0$ interval is modified in the presence of an electric field because of the Stark effect. Such electric fields can arise from motional fields, $(\boldsymbol{v}\wedge\boldsymbol{B})/c$ where $\boldsymbol{v}$ is the beam velocity and $\boldsymbol{B}$ is, say, the Earth's magnetic field, or from residual space charge in the beam.

To determine the correction to the line centre the Stark shift for each level is first evaluated using perturbation theory. Thus for the $|2^2S_{\frac{1}{2}}\,00\rangle$ state (using a $|2^2S_J\,FM_F\rangle$ notation):

$$\delta E_s = \mathrm{Re}\sum_J \sum_{M_F} \frac{|\langle 2^2P_J\,1M_F'|-\boldsymbol{\mu}.\boldsymbol{\mathscr{E}}|\,2^2S_{\frac{1}{2}}\,10\rangle|^2}{E(2^2S_{\frac{1}{2}}\,00)-E(2^2P_J\,1M_F')} \tag{11}$$

and for the $|2^2P_{\frac{1}{2}}\,10\rangle$ state

$$\delta E_p = \mathrm{Re}\sum_{M_F'} \frac{|\langle 2^2S_{\frac{1}{2}}\,1M_F'|-\boldsymbol{\mu}.\boldsymbol{\mathscr{E}}|2^2P_{\frac{1}{2}}\,10\rangle|^2}{E(2^2P_{\frac{1}{2}}\,10)-E(2^2S_{\frac{1}{2}}\,1M_F')}, \tag{12}$$

where Re stands for real part (the energies E are complex to allow for damping), $\boldsymbol{\mathscr{E}}$ the electric field and $\boldsymbol{\mu}$ the electric dipole operator.

In the case of the $(\boldsymbol{v}\wedge\boldsymbol{B})/c$ electric field (where $\boldsymbol{B}$ is the Earth's magnetic field) only the x component of $\boldsymbol{\mu}$ need be considered because $\boldsymbol{v}$, $\boldsymbol{B}$ and the z axis (as defined by the radio-frequency field) lie in the same plane. Hence by expressing μ_x in terms of μ_+ and μ_-, i.e. $\mu_x = \frac{1}{2}(\mu_+ + \mu_-)$,

the two equations become on evaluation of the matrix elements and convertion to frequency units:

$$\delta\nu_s = \left[\frac{\boldsymbol{v}\wedge\boldsymbol{B}\sqrt{6ea_0}}{2hc}\right]^2 \mathrm{Re}\sum_{M'\neq 0}\left(\frac{1}{\nu(2^2\mathrm{S}_{\frac{1}{2}}00)-\nu(2^2\mathrm{P}_{\frac{1}{2}}1M'_F)}+\frac{2}{\nu(2^2\mathrm{S}_{\frac{1}{2}}00)-\nu(2^2\mathrm{P}_{\frac{3}{2}}1M'_F)}\right) \quad (13)$$

where a_0 is the Bohr radius, e the electronic charge, h Planck's constant and c the velocity of light.

$$\delta\nu_p = \left[\frac{\boldsymbol{v}\wedge\boldsymbol{B}\sqrt{6ea_0}}{2hc}\right]^2 \mathrm{Re}\sum_{M'\neq 0}\left(\frac{1}{\nu(2^2\mathrm{P}_{\frac{1}{2}}10)-\nu(2^2\mathrm{S}_{\frac{1}{2}}1M'_F)}\right). \quad (14)$$

The effect of the Stark shift is to increase the interval between the levels being measured, and so the correction becomes $-(\delta\nu_s+\delta\nu_p)$ which on evaluation is $-3.566\sin^2\theta\,\mathrm{THz/T^2}$. Under the conditions of the experiment ($v = 2\times10^8\,\mathrm{cm\,s^{-1}}$, $B = 35\,\mu\mathrm{T}$, and the included angle θ between the field and the beam velocity is 70°) the correction to the nearest kHz is $-4\,\mathrm{kHz}$.

The radial field associated with the residual charged beam may be estimated from:

$$\mathscr{E}_r = \frac{2I}{vr}\times 9\times10^{11}\,\mathrm{V/cm}. \quad (15)$$

The measured beam current I of 2 μA in the interaction region and the beam radius $r = 0.15\,\mathrm{cm}$ give a radial field of about $0.13\,\mathrm{V\,cm^{-1}}$. By comparing this with the $(\boldsymbol{v}\wedge\boldsymbol{B})/c$ electric field of $0.6\,\mathrm{V/cm^{-1}}$, it is seen that the correction due to the space charge field is negligible.

5.4. *Shifts due to emitted Lyman-α radiation*

Within the transition region there is a comparatively large Lyman-α flux caused by the decay of the quenched atoms. Assuming a 100 μA proton beam, and a 5 % production efficiency of metastables, then the maximum production rate of Lyman-α would be 10^{14} photons $\mathrm{s^{-1}}$. Now even if all of this radiation was produced within a 10 mm cube inside the interaction region, the maximum flux of radiation would be only $0.3\,\mathrm{W\,m^{-2}}$ which corresponds to an r.m.s. electric field of $0.1\,\mathrm{V\,cm^{-1}}$. This radiation can cause direct stimulated transitions $2\mathrm{P}\rightleftharpoons 1\mathrm{S}$ in competition with the spontaneous radiation and distorts the line shape; however, the transition rate due to this process is less than 10^{-4} of the spontaneous rate and contributes negligibly to the quench. Lyman-α radiation can also cause a Bloch–Siegert or 'light shift'; however, this is very small (less than 1 Hz).

5.5. *Zeeman effect*

In the weak magnetic field of the Earth the Zeeman effect on the $2^2\mathrm{S}_{\frac{1}{2}}\,F=0\;M_F=0$ to $2^2\mathrm{P}_{\frac{1}{2}}\,F=1\;M_F=0$ interval can be adequately evaluated using second-order perturbation theory. The angle between the magnetic field and the z axis defined by the microwave electric field is such that 94 % of the field is directed along the z axis, and so only the z component of the Zeeman operator is considered. It is obvious, since $M_F = 0$ states are being considered, that there is no first-order contribution, and so for the required accuracy (nearest kHz) only the second-order electron contribution is evaluated. In terms of the matrix elements of the Zeeman operator

$$\mathscr{H}_z = -\mu_\mathrm{B}B(g_l L_z + g_s S_z), \quad (16)$$

the Zeeman shifts δE_s and δE_p in the energies of the $|2^2\mathrm{S}_{\frac{1}{2}}10\rangle$ and $|2^2\mathrm{P}_{\frac{1}{2}}00\rangle$ states are then given by

$$\delta E_\mathrm{s} = \frac{|\langle 2^2\mathrm{S}_{\frac{1}{2}}10|\,\mathscr{H}_z|2^2\mathrm{S}_{\frac{1}{2}}00\rangle|^2}{E(2^2\mathrm{S}_{\frac{1}{2}}00)-E(2^2\mathrm{P}_{\frac{1}{2}}00)} \quad (17)$$

and

$$\delta E_\mathrm{p} = \frac{|\langle 2^2\mathrm{P}_{\frac{1}{2}}00|\,\mathscr{H}_z|2^2\mathrm{P}_{\frac{1}{2}}10\rangle|^2}{E(2^2\mathrm{P}_{\frac{1}{2}}10)-E(2^2\mathrm{P}_{\frac{1}{2}}00)} \quad (18)$$

(μ_B is the Bohr magneton). In this case it is not necessary to take the real part of the expressions above (as was the case for the Stark shift) since the energies appearing in a particular denominator have the same damping constant.

Taking $g_l = -1$ and $g_s = -2$, and noting that the effect of the magnetic field is to reduce the interval being measured, the correction $-\delta E_s + \delta E_p$ to the line centre becomes, on convertion to frequency units,

$$\left(\frac{\mu_B B}{h}\right)^2 \left(\frac{-1}{\nu(2^2S_{\frac{1}{2}}\,00) - \nu(2^2S_{\frac{1}{2}}\,10)} + \frac{\frac{1}{9}}{\nu(2^2P_{\frac{1}{2}}\,10) - \nu(2^2P_{\frac{1}{2}}\,00)}\right). \tag{19}$$

To sufficient precision the $2^2S_{\frac{1}{2}}$ state hyperfine splitting may be taken as 177.5 MHz (Heberle *et al.* 1956), and for the $2^2P_{\frac{1}{2}}$ state one third of this, giving a correction of $+1.472\,\mathrm{THz/T^2}$. Thus to the nearest kHz the Zeeman correction is $+2$ kHz for $B = 35\,\mu\mathrm{T}$. The components of B perpendicular to z give a negligible contribution (less than 1 kHz).

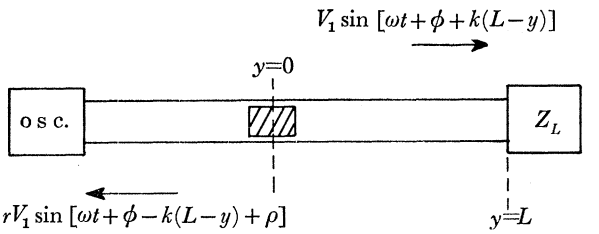

FIGURE 11. Experimental arrangement of microwave components showing forward and reflected waves.

5.6. *Transverse Doppler shift*

The residual first order Doppler effects due to the beam not crossing the radio-frequency travelling wave exactly at right angles are cancelled by reversing the direction of the radio-frequency wave relative to the atomic beam. There is however a second order correction due to the transverse Doppler effect (relativistic time dilation). The atoms move at right angles to the microwave radiation, so that the atomic frequency appears slowed by $(1-v^2/c^2)^{\frac{1}{2}}$. The observed resonance frequency must therefore be increased to correct for this. With a proton beam energy of 21.0 ± 0.1 keV (velocity $2 \times 10^8\,\mathrm{cm\,s^{-1}}$), the correction is $+20$ kHz for an observed frequency of 910 MHz.

5.7. *Shifts due to attenuator and transmission line imperfections*

In order to investigate the effect of reflexions and standing waves in the r.f. measuring system on the resonance centre, consider the typical experimental arrangement shown in figure 11. The radio frequency wave comes from the oscillator on the left, along a transmission line of impedance Z_0 and is absorbed by the load Z_L. If Z_L is not equal to Z_0, some of the power is reflected and the power dissipated in Z_L does not give a true indication of the power at the atomic beam position $y = 0$. If the reflected wave has amplitude rV_1 and a phase advance ρ relative to the incident wave of amplitude V_1, then the mean power $\langle V^2(t)/Z_0 \rangle$ at position $y = L$ is to the first order in r:

$$\langle (V_1^2/Z_0)\,[\sin\{\omega t + \phi + k(L-y)\} + r\sin\{\omega t + \phi - k(L-y) + \rho\}]^2 \rangle$$
$$\approx (V_1^2/2Z_0)\,[1 + 2r\cos\{\rho - 2k(L-y)\}], \tag{20}$$

where $k = \omega/c$ and $\langle\ \rangle$ denotes time average. It is apparent that except at $y = L$, this expression is frequency dependent and would distort a resonance taken with constant power into Z_L. The power meter reading is calibrated for a given forward power, thus the ratio $S(\omega)$ of the total effective power at the beam position $y = 0$ to the power meter reading at $y = L$, i.e. the forward power, may be written:

$$S(\omega) = 1 + 2r\cos(\rho - 2\omega L/c). \tag{21}$$

The effect on the resonance centre of this frequency-dependent power is in general quite complicated, but some insight may be gained by considering the case of a Lorentzian multiplied by the factor $S(\omega)$:

$$\frac{KS(\omega)}{1+[(\omega-\omega_0)/A]^2}, \tag{22}$$

where A is the half-width of the Lorentzian. Now, provided $S(\omega)$ is a slow function of ω, i.e. $2LA/c \ll 1$, then it is possible to perform the Taylor expansion:

$$S(\omega) \approx S(\omega_0) + (\omega - \omega_0)\, G, \tag{23}$$

where $G = (\mathrm{d}S/\mathrm{d}\omega)_{\omega=\omega_0}$, and substitute into (22) to get

$$S(\omega) = \frac{K[1+(\omega-\omega_0)\,G]}{1+(\omega-\omega_0)^2/A^2}. \tag{24}$$

By differentiating and equating to zero we obtain to first order in GA:

$$\omega_{\mathrm{peak}} = \omega_0 + \tfrac{1}{2}GA^2. \tag{25}$$

However we must proceed cautiously for, if instead of differentiating to find the centre, we measure the two half-height frequencies and take the mean, we obtain

$$\omega_{\mathrm{mean}} = \omega_0 + GA^2. \tag{26}$$

This discrepancy just reflects the fact that the resonance, as well as being shifted, is distorted so that the centre value obtained depends on the process used to extract it. This problem was overcome in practice by investigating the values given when the empirical fitting function was used to obtain the 'centre' of a theoretical line shape, calculated assuming a power variation of the type shown in equation (23). The 'centre' was found to be described by an expression:

$$\omega_{\mathrm{centre}} = \omega_0 + \tfrac{1}{2}\beta GA^2, \tag{27}$$

where the constant $\beta \approx 1.77$ for the line shapes corresponding to experimental conditions. The half-width A is that obtained *without* saturation broadening ($0.3125 \times 10^9\ \mathrm{s}^{-1}$).

The effect on the resonance centre of the reflected waves may now be calculated, using equations (21), (23) and (27) to give for the shift $\delta\omega$:

$$\delta\omega = \left(\frac{\beta A^2}{2\omega_0}\right) 2r\left(\frac{2\omega_0 L}{c}\right)\left[\sin\left(\rho - \frac{2\omega_0 L}{c}\right)\right]. \tag{28}$$

This formula was again verified by computer simulations: for $L < 15$ cm and for the typical radio-frequency power of 2 W, the shift to a 910 MHz resonance is:

$$\delta\nu = \frac{\delta\omega}{2\pi} = 5.26r\left\{\left(\frac{2\omega_0 L}{c}\right)\sin\left[\rho - \frac{2\omega_0 L}{c}\right]\right\}\mathrm{MHz}. \tag{29}$$

PHILOSOPHICAL TRANSACTIONS OF THE ROYAL SOCIETY A MATHEMATICAL, PHYSICAL & ENGINEERING SCIENCES

Measurements of the voltage standing wave ratio (v.s.w.r.) of the complete line are displayed in figure 12. The high precision part of these data was obtained by the microwave standards laboratory EQD Aquila; the data are seen to be consistent within the quoted errors, and show no systematic difference when the direction of the r.f. is reversed (open and solid symbols in figure 12). We have also drawn in a suggested fitted line, corresponding to two reactive reflexions $r = 0.0035 f_G$ and $r = 0.001 f_G$, distant 7.5 cm apart (f_G is the frequency in GHz). This appears to describe the behaviour reasonably well, but leaves uncertainties in r of order $0.001 f_G$. Indeed from both experimental and theoretical considerations we would expect terms of this order to be present. For the purposes of this experiment, we have included corrections for all the calculable

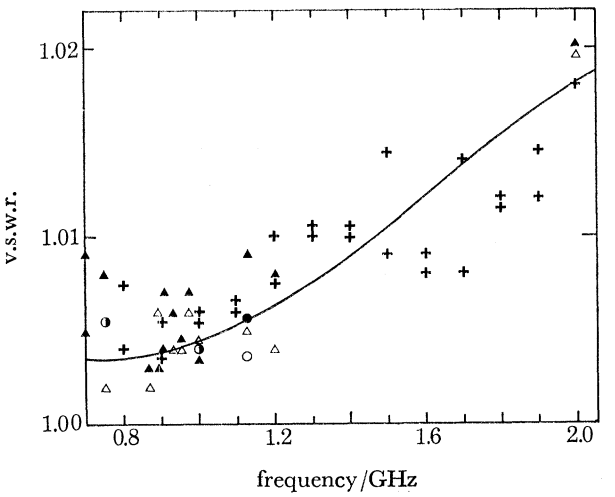

FIGURE 12. Plot of measured v.s.w.r. of complete slab line obtained by (*a*) conventional slotted line techniques (triangles), 2σ error $= \pm 0.005$ (<1 GHz), ± 0.010 (>1 GHz); (*b*) comparison of slab line plus load against reference air lines (circles), 2σ error $= \pm 0.003$; (*c*) comparison of slab line against substituted air line of same electrical length (crosses), 2σ error $= \pm 0.008$. Measurements (*a*) and (*b*) were performed by EQD Aquila Laboratory. The solid line is a fitted curve: v.s.w.r. $= 1 + f_G\,[0.007 + 0.002 \cos \pi f_G]$, where f_G is the frequency in GHz.

effects which we know contribute to the v.s.w.r. and have then assumed that the residual v.s.w.r. is due to shortcomings in the design and construction of the main discontinuities only, and so may be written in the form of the fitted curve in figure 12. Finally the v.s.w.r. of the attenuator was measured and its effect calculated. Thus the corrections applied were as follows:

(*a*) By careful remeasurement of the dimensions of the slab line and coaxial feeders, it was found that the impedance of these were 0.4 % high ($r = 0.002$). From equation (29) it was calculated that this would produce a shift $\delta\nu = -2$ kHz.

(*b*) Placing the compensation gap for the dielectric bead in the slab line rather than in the coaxial region introduced a capacity compensation error ($r = 0.006$) which contributed ± 12 kHz.

(*c*) The residual v.s.w.r. of the line at 910 MHz given in figure 12, interpreted as uncancelled reactances at the main coaxial slab line transition, gives $\delta\nu = \pm 6$ kHz.

(*d*) Finally the attenuator was found to have a v.s.w.r. of 1.002 at 910 MHz, and from the linear increase of r with frequency it was inferred that this was due to an uncancelled reactance in the unit. Use of time domain reflectometry (pulse reflexion) techniques allowed us to determine its

position (3.45 cm from the connector plane), but not its sign. The correction for this effect was determined to be ± 10 kHz.

A summary of these corrections is given in table 3. The values quoted are in effect r.m.s. estimates, since although the modulus of the correction has been measured, the sign of the phase is unknown. An alternative approach, which in this case gives the same result, is to assume that the phase is completely unknown, and so take $(\delta\nu)_{\mathrm{rms}} = \langle \delta\nu^2(\rho)\rangle^{\frac{1}{2}}_{\text{averaged over }\rho} = \sqrt{\frac{1}{2}}(\delta\nu)_{\max}$.

These corrections have been added quadratically to yield an overall correction to be added to the observed resonance frequency of (2 ± 14) kHz for the line and (0 ± 10) kHz for the attenuator. This assumes that the effects are uncorrelated, which may not be strictly true because effects (*a*) and (*b*) might have been absorbed into the final observed v.s.w.r. (effect (*c*)). This would however *reduce* the final uncertainty in the line centre; thus we consider that the r.m.s. sum is a fair, if somewhat cautious, estimate of the total (1σ) uncertainty due to the v.s.w.r.

TABLE 3. SUMMARY OF CORRECTIONS DUE TO V.S.W.R. OF TRANSMISSION LINE AND ATTENUATOR

source	r	L/cm	ρ	correction $-\delta\nu$/kHz
(*a*) correction for actual dimensions of line	0.0007	4.4	0	+6
	0.0024	7.95	π	−4
				+2
(*b*) dielectric bead compensation error	0.006	4.4	$\pm\pi/2$	± 5
	0.006	4.9	$\mp\pi/2$	∓ 17
				+12
(*c*) residual uncancelled capacity at transitions	0.003	4.4	$\pm\pi/2$	± 6
(*d*) attenuator reactance	0.001	11.2	$\pm\pi/2$	± 10

5.8. *Corrections for power meter and attenuator efficiency*

The r.f. power measuring system consisted of a General Radio 10 dB attenuator, a GR900 to APC-7 adaptor and a Hewlett–Packard type 8481A power measuring head and type 435A power meter. The frequency response of the complete system, attenuator plus power head, was measured by EQD Aquila Laboratory (private communication), using reference standards directly traceable to U.K. prime standards. The measured calibration factor is shown in figure 13; we have attempted to draw a smooth curve through the points to determine the slope G at 910 MHz, and find $G = (0.5 \pm 0.5) \times 10^{-6}\,\mathrm{MHz}^{-1}$. Using equation (27) (§ 5.7) we calculate that this corresponds to a correction $-\delta\nu = (-1 \pm 1)$ kHz.

5.9. *Frequency dependence of skin resistance*

To calculate the effective power at the beam position half-way along the transmission line, relative to the power absorbed at the load, it is necessary to calculate the attenuation of the line itself due to the skin resistance. The resistance per unit length r of a cylindrical conductor at high frequency is given by

$$r = \frac{1}{2\pi R\sigma\delta_{\mathrm{s}}}, \tag{30}$$

where R is the radius of the conductor (3.1 mm) and σ the conductivity of the material. The skin depth δ_s is given by

$$\delta_s = \left(\frac{2}{\omega\mu\sigma}\right)^{\frac{1}{2}}, \tag{31}$$

where ω is the angular frequency and μ the permittivity (equal to $\mu_0 = 4\pi \times 10^{-7} H\,m^{-1}$). For aluminium $\sigma = 3.8 \times 10^7\,\Omega^{-1}\,m^{-1}$, giving $\delta_s = 2.5\,\mu m$ at 1 GHz and $r = 0.15\,\Omega\,m^{-1}$.

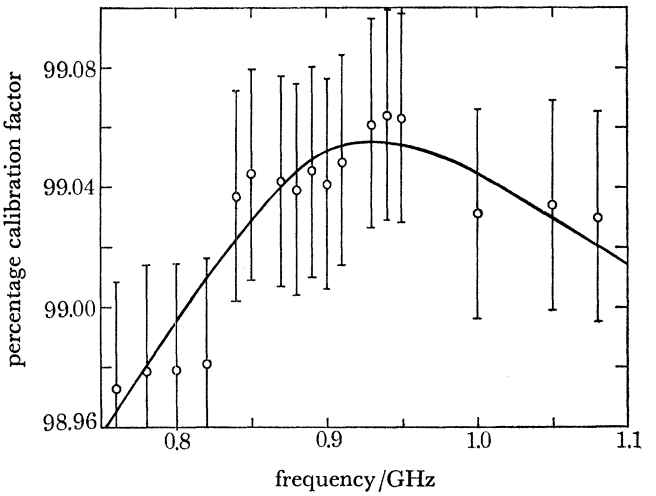

FIGURE 13. Frequency dependence of the calibration factor for the HP8481A microwave power measuring head and attenuator.

The attenuation of a voltage wave travelling along this line takes the form:

$$V(y) = V_0 \exp[-(ry/2Z_0)], \tag{32}$$

where Z_0 is the characteristic impedance of the line. The dominant contribution to the attenuation comes from the centre conductor only, the other conductor having a much larger surface area and effective R.

Expansion of the exponent to first order gives for the power

$$\frac{|V(y)|^2}{Z_0} = \frac{V_0^2}{Z_0}\left(1 - \frac{2ry}{2Z_0}\right) = \rho_0(1 - 6 \times 10^{-4} f_G^{\frac{1}{2}}) \tag{33}$$

if $y = 60$ mm and f_G is the frequency in GHz. The frequency dependent power slope across the resonance is thus calculated by differentiation to be

$$\tfrac{1}{2} \times 6 \times 10^{-4} \times 10^{-3} = 0.3 \times 10^{-6}\,MHz^{-1} \tag{34}$$

which produces a shift of less than 1 kHz ($+0.7$ kHz).

5.10. *Frequency dependence of on–off ratio*

The on–off ratio of the PIN modulator r.f. switch was measured and found to be frequency dependent. As well as a steady slow decrease with frequency, there were small periodic variations every 60 MHz, probably due to standing waves in the connecting cables. The fluctuations over the frequency range 850–970 MHz were within ± 0.5 dB of 38.2 dB and corresponded to a possible slope of less than $0.2 \times 10^{-6}\,MHz^{-1}$, or a shift of 0.5 kHz.

5.11. *Oscillator harmonics*

The presence of harmonics in the oscillator output would lead to discrepancies between the measured power and the power component stimulating the resonance transitions (the fundamental only). The spectral output of the oscillators was measured using a type 141T Hewlett–Packard spectrum analyser. It was found that the oscillator output itself had harmonics (particularly third and fifth) only about 30 dB down on the fundamental. However, the signal actually reaching the transmission line was considerably filtered by the circulators, making these frequency components unmeasurably small (> 50 dB down).

The possibility was investigated that the higher harmonics, though very small, might be artificially enhanced by exciting a resonant cavity mode of the slab line, thus causing $2^2S_{\frac{1}{2}}$–$2^2P_{\frac{3}{2}}$ fine structure transitions at 10 028 MHz. By careful investigation of the quench around 1114 MHz, i.e. $\frac{1}{9}$ of this frequency interval, it was possible to ascertain that such a resonance was certainly more than 10^3 smaller than the main resonance and so contributed negligible shift.

5.12. *Correction and calibration of the measured oscillator frequency*

In the process of taking the data it was noticed that the frequency of the oscillators varied quite appreciably with their loading, in particular on whether the r.f. switch was open or closed. The circulators greatly reduced the effect, but even so the frequency measured when the switch was 'on' could differ from the frequency with r.f. 'off' by up to 40 kHz. These errors were, however, roughly equally divided between positive and negative, so that the overall effect on the resonance centre is much less than this. This was investigated by fitting theoretical data, which had been 'doctored' to simulate these frequency mis-measurements. The results showed that a correction of -0.001 MHz should be applied. The calibration of the frequency counter was also checked against a broadcast standard frequency locked to an atomic clock time standard, and found to be accurate to $0.1/10^6$.

5.13. *Residual effect of the $F = 1$ levels*

After the experimental data had been fitted to the sum of three resonance line shapes (as described in § 4.3), the data were re-examined to see if there was any systematic dependence of the observed Lamb shift values on the strength of the weak $F = 1$ resonances. We therefore define a parameter

$$\eta = \frac{\text{sum of } F = 1 \text{ resonance amplitudes}}{F = 0 \text{ resonance amplitude}} = \frac{a_2 + a_3}{a_1}, \tag{35}$$

which depends on the microwave power levels in the state-selector and main transition region. We tried fitting the experimental Lamb shifts obtained to the linear function $a\eta + b$. The intercept b, which corresponds to extrapolating to zero $F = 1$ component, was found to be 1057.827 and 1057.847 for the data sets given in tables 1 and 2, that is, $+0.004$ MHz above the simple weighted mean values 1057.823 and 1057.843 respectively. The error associated with this correction is however also ± 0.004 MHz, which indicates that the correction is not significantly non-zero and the original fitting process accommodates the $F = 1$ resonances reasonably well.

5.14. *Effects due to $n = 4$ metastable atoms*

In the charge exchange process, atoms are created in many different quantum states, but of these only the 2s state has a lifetime greater than 1 μs. However, it is important to consider whether

it is possible for atoms in other states to reach the detector, and produce a signal dependent on the microwave frequency.

The only states having allowed electric dipole transitions within the frequency range used in the experiment are the $4^2S_{\frac{1}{2}}$ (lifetime 230 ns) and the $4^2F_{\frac{5}{2}}$ (73 ns) states (Lundeen 1975). These can cause resonances at the following frequencies:

$4s_{\frac{1}{2}}$–$4p_{\frac{3}{2}}$ 1239 MHz (single photon),

$4f_{\frac{5}{2}}$–$4p_{\frac{1}{2}}$ 912 MHz (double photon),

$4s_{\frac{1}{2}}$–$4d_{\frac{5}{2}}$ 847 MHz (double photon).

(These lines are in fact split by the hyperfine interaction, but due to the larger electric dipole matrix elements found for $n = 4$ states, the saturation broadening is sufficient to mask this splitting.)

The flight time between the charge exchange and interaction regions is 700 ns. Thus, if we assume the initial level populations to be proportional to $1/n^3$ and that we lose three-quarters of 2s atoms but few of the 4s and 4f atoms in the state selector, then we obtain for the populations entering the interaction region (relative to the 2s beam):

4s 0.025,

4f 3×10^{-5},

4p, 4d $< 10^{-7}$.

These represent upper limits on the signal which would appear at the detector. Indeed a more detailed treatment including plausible assumptions about the behaviour of the detector, indicates that the observed r.f. dependent signal would be 3 % of those figures, in which case 4s resonances of 0.1 % may well be present.

To gain more information, the residuals obtained after individual fitting of the experimental runs were pooled and after subtracting the residuals obtained for the theoretical line shape (figure 8) the pattern shown in figure 14 (*a*) was obtained. This clearly shows an additional feature in the neighbourhood of 1.2 GHz. The effect of this additional resonance was estimated by fitting a theoretical line shape consisting of a $n = 2$ line shape plus an additional $n = 4$ line shape centred on 1.239 GHz using the usual empirical fitting function, and noting the shift and distortion produced as a function of the $n = 4$ amplitude. An $n = 4$ line shape at 1239 MHz was then fitted to the observed residuals to determine the $n = 4$ amplitude in the experimental data. The best fit for the amplitude $(3.6 \pm 1.5) \times 10^{-4}$ corresponds to a shift of $+(2 \pm 1)$ kHz and leaves the residuals shown in figure 14 (*b*).

Though the fit as measured by the χ^2 test is sufficiently good, it is necessary to repeat the process for the 847 MHz resonance, because this is also due to $4^2S_{\frac{1}{2}}$ atoms, and so would be expected to be apparent. The result of the fitting is an amplitude $(2.2 \pm 1.4) \times 10^{-4}$, and an additional shift of $-(9 \pm 5)$ kHz, leaving the residuals in figure 14 (*c*). The effect of fitting a resonance at 915 (due to the 4f state) was also ascertained. This gave for the amplitude a value $(-1.7 \pm 3.3) \times 10^{-4}$, which is not incompatible with the expected value of less than 10^{-5}; it has therefore been neglected. The combined result for the correction due to the $n = 4$ levels is thus $(+7 \pm 5)$ kHz.

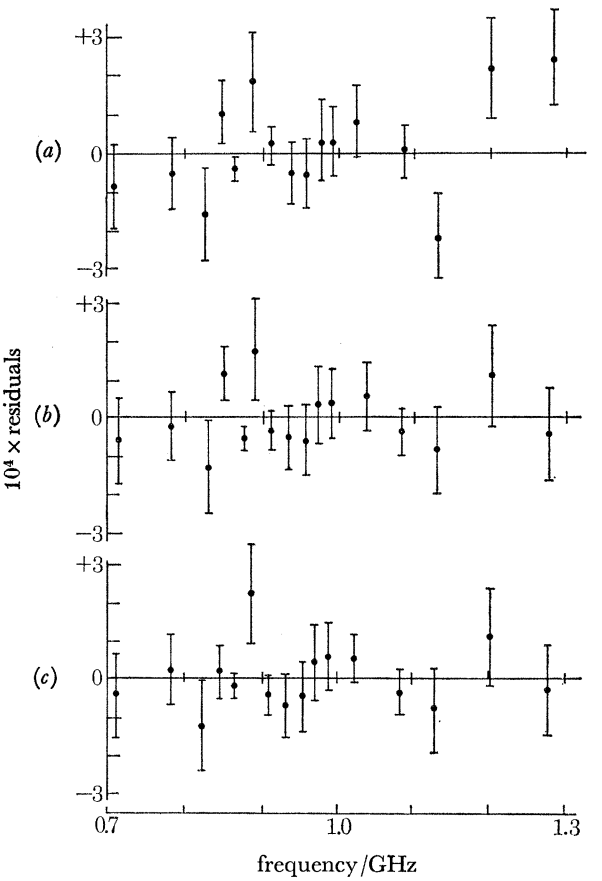

FIGURE 14. (*a*) Pooled residuals obtained from the fitted data minus the residuals obtained by fitting computer simulated data. (*b*) The result after having fitted to the pooled residuals a $4^2S_{\frac{1}{2}}$–$4^2P_{\frac{3}{2}}$ resonance centred at 1239 MHz. (*c*) The result after fitting to the pooled residuals a further resonance centred at 847 MHz, $4^2S_{\frac{1}{2}}$–$4^2D_{\frac{3}{2}}$.

TABLE 4. RESULTS AND SYSTEMATIC CORRECTIONS

Values in MHz	magnitude ($\pm 1\sigma$)
weighted mean of experimental runs (including individual Bloch–Siegert shift and hyperfine structure addition†)	1057.823 ± 0.011 (normal) 1057.843 ± 0.011 (reversed)
	1057.833 ± 0.008
transverse Doppler shift	+ 0.020 ± 0.000
power meter and attenuator frequency dependence	− 0.001 ± 0.001
frequency calibration	− 0.001 ± 0.001
v.s.w.r. of slab line	+ 0.002 ± 0.014
v.s.w.r. of attenuator	0.000 ± 0.010
Zeeman effect	+ 0.002 ± 0.000
residual effect of $F = 1$ resonances	+ 0.004 ± 0.004
effect of $n = 4$ resonances	+ 0.007 ± 0.005
Stark shift due to residual 2μA proton bean	− 0.000 ± 0.000
($\boldsymbol{v} \wedge \boldsymbol{B}$) Stark shift	− 0.004 ± 0.000
final Lamb shift	1057.862 ± 0.020
hyperfine addition†	− 147.958
$2^2S_{\frac{1}{2}}$ $F = 0$, $2^2P_{\frac{1}{2}}$ $F = 1$ interval	909.904 ± 0.020

† The hyperfine addition was calculated using eqns. (6), (8) and (10*a*) of Brodsky & Parsons (1967) which include anomalous moment and relativistic corrections. We note that our result differs from that given by Lundeen & Pipkin (1975) by 0.005 MHz.

6. Discussion

6.1. *Results*

The experimental corrections are summarized in table 4. The uncertainties quoted there are intended to be realistic one standard deviation (1σ) estimates, and not absolute 'limits of error' (2 or 3σ). They were obtained wherever possible from repeated measurements by statistical techniques. The errors have been added quadratically to give a total systematic error estimate of ± 0.018 MHz, which, when combined with the total statistical (counting) error (± 0.008 MHz), gives for the total estimated error for the measurement ± 0.020 MHz. A number of comments can be made about this result.

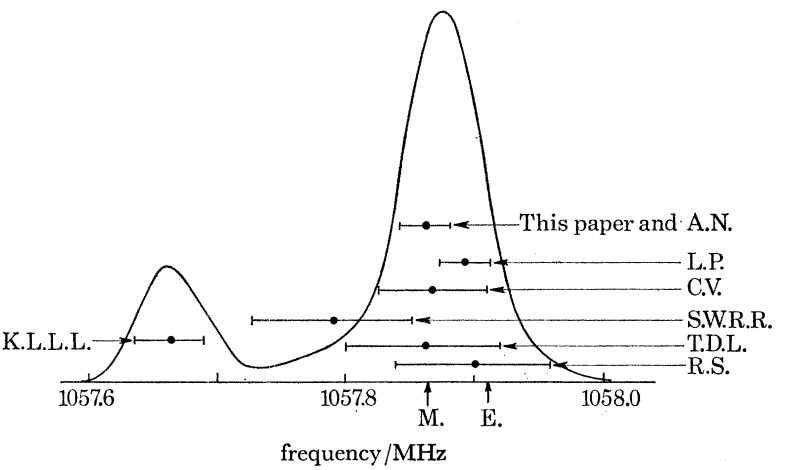

Figure 15. Our measurement and previous microwave measurements plotted as an ideogram. The positions of the calculated values of Mohr & Erickson are marked by the arrow heads. K.L.L.L., Kaufman *et al.* (1969); S.W.R.R., Shyn *et al.* (1969); T.D.L., Triebwasser *et al.* (1953) revised in accordance with Robiscoe & Shyn (1970); A.N., Andrews & Newton (1976); C.V., Cosens B. L. & Vorburger, T. V. (1969); L.P., Lundeen & Pipkin (1975); R.S., Robiscoe & Shyn (1970).

First, the statistical error hardly contributes to the final uncertainty, which is dominated by the systematic r.f. measurement uncertainties (± 0.017 MHz). Secondly, the final error (± 0.020 MHz) is only half the statistical uncertainty associated with a *single* run; this means that we are not relying greatly on a large number of runs for a statistical reduction in the uncertainty. This is important when as here the error estimate associated with each run contains a component due to the fitting process itself. This was estimated to be 0.005 MHz, which if separated out from the individual run uncertainties and then added to the revised error in the mean, would only increase the total statistical error from 0.008 to 0.009 MHz and have negligible effect on the final answer.

Thirdly, it might be noted that the actual magnitude for the majority of the corrections is relatively small (< 0.020 MHz), the only exceptions being the transverse Doppler shift and the Bloch–Siegert shift. The former is purely kinetic and well understood; the latter has been verified experimentally for single quantum transitions (Andrews & Newton 1975) and much more precisely (1%) for triple quantum transitions (Andrews & Newton 1976*c*). Finally we can summarize the above by saying that we are confident that no *known* uncertainty is likely to shift the final answer by more than 40 kHz (95% confidence level).

6.2. *Comparison with previous measurements*

We now compare our result with previous measurements. In figure 15 we have plotted an ideogram (see Particle Data Group 1976) of recent high precision measurements. (Each point is represented by a gaussian error curve of amplitude $1/\sigma^2$ and width σ, and the curves added to give the overall ideogram, or probability curve.) These have in the most part been taken from the recent review by Erickson (1977) and include both direct ($2S_{\frac{1}{2}}$–$2P_{\frac{1}{2}}$) and indirect ($2S_{\frac{1}{2}}$–$2P_{\frac{1}{2}}$) measurements, the latter being incorporated by subtracting the theoretical value of the fine structure interval (Erickson 1977) using $\alpha^{-1} = 137.035987$ (Olsen & Williams 1975). It is apparent that, with the exception of a single result, the measurements are reasonably consistent, and in particular our new value is in good agreement with the previously most precise value of Lundeen & Pipkin (1975). The discrepant measurement (Kaufman *et al.* 1969) is perhaps significantly the only one of the experiments not to use an atomic beam, but the 'magnetic bottle' method instead. The remaining measurements, performed over the last 25 years, by different groups using various techniques, present a clear and self-consistent picture.

6.3. *Comparison with theory*

We now consider the comparison with theory. Lamb shift calculations since the first pioneering paper by Bethe (1947) have undergone considerable refinement, which has not always been accompanied by improved agreement with experiment. However, after the recalculation by Appelquist & Brodsky (1970) of the fourth-order self-energy contribution previously calculated analytically by Soto (1966), agreement was obtained with the then most recent experiments. The full Lamb shift calculation has been refined most recently by Erickson (1971, 1977) and yields a value 1057.910 ± 0.010 MHz. However, a recent numerical calculation on high Z hydrogenic ions by Mohr (1975) has cast doubt on the second-order binding corrections previously calculated by Erickson. Further, by extrapolating his results to the case of $Z = 1$ Mohr calculates a value 1057.864 ± 0.014 MHz, significantly lower than the Erickson result.

We have also indicated these two theoretical predictions on figure 15. It is apparent that the experimental evidence favours Mohr's value. In particular, the present experiment is in very good agreement with this value, but in distinct disagreement with Erickson's value (difference -0.048 ± 0.024 MHz). If we calculate the goodness of fit χ^2 for all the experimental results (except Kaufman *et al.* 1969) with respect to the two theories we obtain 5.15 for Mohr and 13.13 for Erickson, with six degrees of freedom. The former figure is quite reasonable but the second is only just within the 95% confidence limits.

Recently a further complication has arisen which modifies the theoretical predictions somewhat (Andrews *et al.* 1977). Amongst the terms contributing to the 2S–2P energy difference is that due to the finite size of the proton. This contributes about 125 kHz and is proportional to the square of the proton radius, a quantity normally obtained from electron–proton scattering experiments. Recently these experiments have been re-analysed by the Bonn group (Borkowski *et al.* 1974; Höhler *et al.* 1976) who obtain substantially larger values for the proton radius. If those new values are used instead of the previously accepted value of Hand *et al.* (1963), then the Lamb shift is increased by up to 20 kHz. Such an increase would, however, only increase the discrepancy with Erickson's values without substantially affecting the agreement between Mohr's values and experiment.

6.4. *Conclusion*

Our measurement of the $n = 2$ Lamb shift in hydrogen using a fast atomic beam is capable, unlike previous measurements, of discriminating between two rival theoretical predictions, and supports that of Mohr. We now consider possible future developments. It was noted in § 6 that the limiting factor to the precision of the final result is uncertainty in the r.f. measurements. This could (in principle) be reduced by constructing a transition region with still lower v.s.w.r. However we are approaching the limit of that which is measurable, and it is difficult to envisage an improvement of more than a factor of 2. The r.f. power measurement problem may, however, be circumvented by using an auxiliary calibration atomic beam (Andrews & Newton 1977) which could lead to a result with an uncertainty of 5 kHz. An additional possibility would be a measurement of the deuterium Lamb shift which is known only relatively imprecisely (Cosens 1968). The problems of line shape analysis are appreciably more severe in this case, however, due to competing overlapping resonances caused by the smaller hyperfine structure, which make state selection less effective.

Recent interest has also been expressed in purely leptonic atoms (positronium, muonium, etc.). The appeal of these systems is that they may be calculated completely *ab initio* without reliance on measured nuclear form factors. For example, the $n = 2$ fine structure interval in positronium has recently been measured (Mills *et al.* 1975) and the precision of both experiment and theory will doubtless improve in the future. However, owing to their ease of preparation and detection, hydrogenic systems will remain the premier test of atomic structure theories for some time to come.

The authors would like to thank E.Q.D. Aquila Microwave Standards Laboratory for their assistance in calibrating the precision transmission line; Messrs B. Butlin, M. Jarvis, J. Osborne and F. Schofield for their excellent work in constructing the apparatus; Messrs N. Cooper, A. MacKenzie and D. Newell of the University's Computing staff for their valuable advice; Professor K. F. Smith for his encouragement and interest; the Science Research Council for a grant and a Research Studentship for D. A. Andrews and the Royal Commission for the Exhibition of 1851 for a Research Fellowship for G. Newton. Finally the authors would like to thank R. Bolton for proof-reading the manuscript.

References

Andrews, D. A., Golub, R. & Newton, G. 1977 *J. Phys.* G **3**, L91.
Andrews, D. A. & Newton, G. 1975 *J. Phys.* B **8**, 1415.
Andrews, D. A. & Newton, G. 1976*a* *Phys. Rev. Lett.* **37**, 1254.
Andrews, D. A. & Newton, G. 1976*b* *J. Phys.* B **9**, 1453.
Andrews, D. A. & Newton, G. 1976*c* *Phys. Lett.* **57** A, 417.
Andrews, D. A. & Newton, G. 1977 *J. Phys.* B **10**, 2333.
Appelquist, T. & Brodsky, S. J. 1970 *Phys. Rev. Lett.* **24**, 562.
Bethe, H. A. 1947 *Phys. Rev.* **72**, 339.
Bloch, F. & Siegert, A. 1940 *Phys. Rev.* **57**, 522.
Bohr, N. 1913 *Phil. Mag.* **26**, 1.
Bohr, N. 1915 *Phil. Mag.* **29**, 332.
Borkowski, F., Peuser, P., Simon, G. G., Walther, V. H. & Wendling, R. D. 1974 *Nucl. Phys.* A **222**, 269.
Brodsky, S. J. & Parsons, R. G. 1967 *Phys. Rev.* **163**, 134.
Brodsky, S. J. & Parsons, R. G. 1968 *Phys. Rev.* **176**, 423.

PHILOSOPHICAL TRANSACTIONS OF THE ROYAL SOCIETY A MATHEMATICAL, PHYSICAL & ENGINEERING SCIENCES

Cosens, B. L. 1968 *Phys. Rev.* **173**, 49.
Cosens, B. L. & Vorburger, T. V. 1969 *Phys. Rev. Lett.* **22**, 1273.
Dirac, P. A. M. 1928 *Proc. R. Soc. Lond.* A **117**, 610.
Drinkwater, J. W., Richardson, O. & Williams, W E 1940 *Proc. R. Soc. Lond.* A **174**, 164.
Erickson, G. W. 1971 *phys. Rev. Lett.* **27**, 780.
Erickson, G. W. 1977 *J. phys. Chem. Ref. Data* **6**, 831.
Erickson, G. W. & Yennie, 1965 *Ann. Phys. New York* **35**, 271 and 447.
Goudsmit, S. & Uhlenbeck, G. E. 1926 *Nature, Lond.* **117**, 264.
Hand, L. N., Miller, D. G. & Wilson, R. 1963 *Rev. mod. Phys.* **35**, 335.
Heberle, J. W., Reich, H. A. & Kusch, P. 1956 *Phys. Rev.* **101**, 612.
Höhler, G., Pietarinen, E., Sabba-Stefanescu, I., Borkowski, F., Simon, G. G., Walther, V. H. & Wendling, R. D. 1976 *Nucl. Phys.* B **114**, 505.
Houston, W. V. & Hsieh, Y. M. 1934 *Phys. Rev.* **45**, 263.
Hughes, V. W. 1960 *Quantum electronics*, ed. C. H. Townes. New York: Columbia University Press.
Kaufman, S. L., Lamb, W. E., Lea, K. R. & Leventhal, M. 1969 *Phys. Rev. Lett.* **22**, 507.
Kopferman, H., Krüger, H. & Ohlmann, H. 1949 *Z. Phys.* **126**, 760.
Kuhn, H. & Series, G. W. 1950 *Proc. R. Soc. Lond.* A **202**, 127.
Lamb, W. E. & Retherford, R. C. 1947 *Phys. Rev.* **72**, 241.
Lamb, W. E., Retherford, R. C., Triebwasser, S. & Dayhoff, E. S.
Part I 1950 *Phys. Rev.* **79**, 549.
Part II 1951 *Phys. Rev.* **81**, 222.
Part III 1952 *Phys. Rev.* **85**, 259.
Part IV 1952 *Phys. Rev.* **86**, 1014.
Part V 1953 *Phys. Rev.* **89**, 98.
Part VI 1953 *Phys. Rev.* **89**, 106.
Liebmann, G. 1949 *Proc. phys. Soc.* **62**(4), 213.
Lundeen, S. R. 1975 Ph.D. thesis, Harvard University, U.S.A.
Lundeen, S. R. & Pipkin, F. M. 1975 *Phys. Rev. Lett.* **34**, 1368.
Mac, J. E. & Austern, N. 1947 *Phys. Rev.* **72**, 972.
Mac, J. E. & Austern, N. 1950 *Phys. Rev.* **77**, 745.
Michelson, A. A. & Morley, E. W. 1887 *Phil. Mag.* **24**, 466.
Mills, A. P., Berko, S. & Canter, K. F. 1975 *Phys. Rev. Lett.* **34**, 1541.
Mohr, P. J. 1975 *Phys. Rev. Lett.* **237**, 780.
Murakawa, K., Suwa, S. & Karmer, T. 1949 *Phys. Rev.* **76**, 1721.
Newton, G. & Unsworth, P. J. 1975 *J. appl. Phys.* **47**, 70.
Newton, G., Unsworth, P. J. & Andrews, D. A. 1975 *J. Phys.* B **8**, 2928.
Olsen, P. T. & Williams, E. R. 1975 *Fifth International Conference on Atomic Masses and Fundamental Constants, Paris.*
Particle Data Group 1976 *Rev. mod. Phys.* **48**, 1S.
Pasternack, S. 1938 *Phys. Rev.* **54**, 1113.
Ramsey, N. F. 1956 *Molecular beams.* England. Oxford University Press.
Robiscoe, R. T. 1965 *Phys. Rev.* **138**, A22.
Robiscoe, R. T. 1968 *Phys. Rev.* **186**, 4.
Robiscoe, R. T. & Cosens, B. L. 1966 *Phys. Rev. Lett.* **17**, 69.
Robiscoe, R. T. & Shyn, T. W. 1970 *Phys. Rev. Lett.* **24**, 559.
Salpeter, E. 1953 *Phys. Rev.* **89**, 92.
Shirley, J. H. 1975 *Phys. Rev.* B **138**, 979.
Shyn, T. W., Williams, W. L., Robiscoe, R. T. & Rebane, T. 1969 *Phys. Rev. Lett.* **22**, 1273.
Smith, W. V. 1943 *J. chem. Phys.* **11**, 110.
Sommerfeld, A. 1916 *Ann. Phys. Lipz.* **51**, 1.
Soto, M. F. 1966 *Phys. Rev. Lett.* **17**, 1153.
Triebwasser, S., Dayhoff, E. S. & Lamb, W. E. 1953 See Lamb *et al.*, Part V.
Unsworth, P. J. 1969 *J. sci. Instrum.* **2**, 407.
Welton, T. A. 1948 *Phys. Rev.* **74**, 1157.
Whinnery, J. R., Jamieson, H. W. & Robbins, T. E. 1944 *Proc. Inst. Radio Engrs* **32**, 695.
Wholey, W. B. & Eldred, W. N. 1950 *Proc. Inst. Radis Engrs.* **38**, 244.
Williams, R. C. 1938 *Phys. Rev.* **54**, 558.

Appendix

Calculation of slab line fields

The slab line geometry is shown in figure 16 (*a*). A circular centre conductor (solid line) held at a potential $\phi = \phi_0$ is midway between two infinite earthed flat sheets at $z = \pm \frac{1}{4}\pi$. By use of

a conformal transformation in the $0xz$ plane (Wholey & Eldred 1950) it is possible to redraw the system in terms of coordinates u and v defined by

$$u+iv = \tan(z+ix). \tag{36}$$

This is done in figure 16 (b). It is apparent that the flat plates have transformed into a cylinder of unit radius, and the centre conductor to an elliptical shape. Now if we are principally interested in evaluating the field near the flat plates in the (z, x) picture (along the actual beam path, for instance), then we may make an approximation in the (u, v) picture by distorting the centre conductor until it is circular, i.e. the broken line in figure 16 (b).

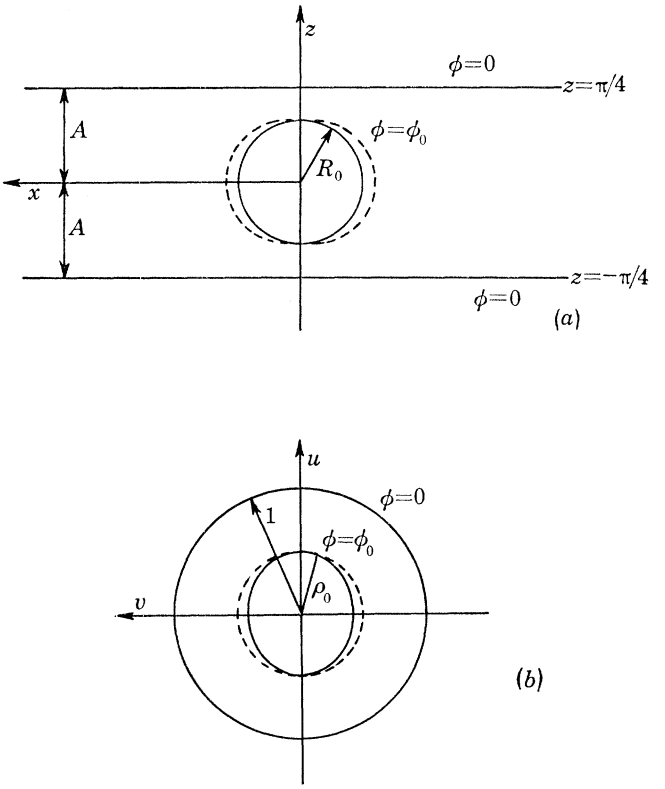

FIGURE 16. (a) Slab line geometry; (b) the redrawn slab line geometry according to the conformal transformation $u+iv = \tan(z+ix)$.

This enables the potential ϕ to be written down directly:

$$\phi = \phi_0 \ln(\rho)/\ln(\rho_0), \tag{37}$$

where $\rho^2 = u^2+v^2$ and $\rho_0 = \tan(\pi R_0/4A)$. The Cartesian field components

$$\mathscr{E}_x = -\frac{\partial\phi}{\partial x}, \quad \mathscr{E}_z = -\frac{\partial\phi}{\partial z} \tag{38}$$

are now evaluated using the transformation equations

$$u = \frac{\tan z \operatorname{sech}^2 x}{1+\tan^2 z \tanh^2 x} \quad v = \frac{\tanh x \sec^2 z}{1+\tan^2 z \tanh^2 x}, \tag{39}$$

which are just the real and imaginary parts of (36). The results are:

$$\mathscr{E}_x = \frac{\mathscr{E}_0(1-\tan^4 z)\,(1-\tanh^2 x)\tanh x}{2\,(\tan^2 z\,\mathrm{sech}^4 x+\tanh^2 x\sec^4 z)}, \tag{40}$$

$$\mathscr{E}_z = -\frac{-\mathscr{E}_0(1+\tan^2 z)\tan z\,(1-\tanh^4 x)}{2\,(\tan^2 z\,\mathrm{sech}^4 x+\tanh^2 x\sec^4 z)}, \tag{41}$$

where

$$\mathscr{E}_0 = \frac{2\phi_0}{\ln[\tan(\pi R_0/4A)]}\left(\frac{\pi}{4A}\right). \tag{42}$$

This approximation is adequate to calculate the fields driving the resonance. However, to obtain the correct impedance for the slab line it is necessary to expand the centre conductor shape in a series of cylindrical harmonics, and calculate the contribution of each of these to the impedance.

PHILOSOPHICAL TRANSACTIONS OF THE ROYAL SOCIETY A MATHEMATICAL, PHYSICAL & ENGINEERING SCIENCES